GeoArabia, 2012, v. 17, no. 3, p. 17-56
Gulf PetroLink, Bahrain

Impact of diagenesis on the spatial and temporal distribution of reservoir quality in the Jurassic Arab D and C members, offshore Abu Dhabi oilfield, United Arab Emirates

Sadoon Morad, Ihsan S. Al-Aasm, Fadi H. Nader,
Andrea Ceriani, Marta Gasparrini and Howri Mansurbeg

ABSTRACT

This study is based on petrographic examination (optical, scanning electron microscope, cathodo-luminescence, backscattered electron imaging, and fluorescence) of 1,350 thin sections as well as isotopic compositions of carbonates (172 carbon and oxygen and 118 strontium isotopes), microprobe analyses, and fluid inclusion microthermometry of cored Jurassic Arab D and C members from 16 wells in a field from offshore Abu Dhabi, United Arab Emirates. The formation was deposited in a ramp with barrier islands and distal slope setting. Petrographic, stable isotopic and fluid-inclusion analyses have unraveled the impact of diagenesis on reservoir quality of Arab D and C within the framework of depositional facies, sequence stratigraphy, and burial history. Diagenetic processes include cementation by grain rim cement and syntaxial calcite overgrowths, formation of moldic porosity by dissolution of allochems, dolomitization and dolomite cementation, cementation by gypsum and anhydrite, and stylolitization. Partial eogenetic calcite and dolomite cementation has prevented porosity loss in grainstones during burial diagenesis. Dolomitization and sulphate cementation of peritidal mud are suggested to have occurred in an evaporative sabkha setting, whereas dolomitization of subtidal packstones and grainstones was driven by seepage reflux of lagoon brines formed during major falls in relative sea level. Recrystallization of dolomite occurred by hot saline waters (T_h 85–100°C; and salinity 14–18 wt% NaCl). Anhydrite and gypsum cements (T_h 95–105°C; fluid salinity 16–20 wt% NaCl), were subjected to extensive dissolution, presumably caused by thermal sulfate reduction followed by a major phase of oil emplacement. The last cement recorded was a second phase of anhydrite and gypsum (T_h 95–120°C; 16–22 wt% NaCl), which fills fractures associated with faults.

INTRODUCTION

The quality and heterogeneity of carbonate reservoirs are inherently challenging to production and to secondary and tertiary recovery, due to the multiple inter-related controlling parameters. These parameters include depositional environments, diagenetic processes, structural evolution, burial-thermal history of the basin, and timing of hydrocarbon emplacement (Stoessel and Moore, 1983; Choquette and James, 1987; Morad, 1998; Wang and Al-Aasm, 2002; Esteban and Taberner, 2003; Wierzbicki et al., 2006). Heterogeneous distribution of primary porosity and permeability in carbonate successions is accentuated by diagenetic alterations, such as cementation, grain dissolution and dolomitization (Wang and Al-Aasm, 2002; Westphal et al., 2004; Esrafili-Dizaji and Rahimpour-Bonab, 2009; Harris, 2010). Diagenetic alterations, which occur at near-surface conditions and during progressive burial, are mediated by advective fluid flow and/or diffusion. Permeable rock units and fractures play an important role in heat and mass transfer during burial diagenesis (Machel et al., 1996; Morad et al., 2000).

Sequence-stratigraphic models can predict depositional facies, and hence primary porosity and permeability distribution (Loucks and Sarg, 1993). However, these models cannot provide direct information about the impact of diagenesis on the evolution of reservoir quality. Most of the controls on early diagenetic processes are also sensitive to relative sea level changes (e.g. pore-water composition and flow, timing and duration of subaerial exposure); thus eogenesis can be linked to sequence stratigraphy (Morad et al., 2011). It is logical to assume that the integration of diagenesis and

sequence stratigraphy will constitute a powerful tool for the prediction of the spatial and temporal distribution and evolution of reservoir quality in carbonate reservoirs (Goldhammer et al., 1990; Tucker, 1993; Moss and Tucker, 1995; Bourque et al., 2001; Eberli et al., 2001; Glumac and Walker, 2002; Tucker and Booler, 2002; Moore, 2001; Caron et al., 2005). This approach can also provide useful information on the formation of diagenetic seals, barriers, and baffles for fluid flow, which may cause compartmentalization of the reservoirs.

The Upper Jurassic Arab Formation, which extends over large parts of the Arabian Gulf region, is considered to be one of the largest oil and gas reservoirs in the world (Beydoun, 1991). However, detailed diagenetic studies linking petrographic, geochemical, and fluid-inclusion data to depositional facies, sequence-stratigraphic frameworks, and the burial-thermal evolution of the basin are still lacking. Material and data of the Arab Formation from 16 wells from an oilfield, offshore Abu Dhabi, United Arab Emirates (Figure 1) were investigated. The objectives of this study are: (1) to unravel the spatial and temporal distribution and conditions of diagenetic alterations, and (2) to develop a conceptual model of the impact of diagenetic alterations on reservoir-quality distribution and evolution pathways. Focus is put on the Arab D and C members, which are the reservoir intervals of the Arab Formation. The geological and sequence-stratigraphic framework as well as the lithological description and interpretation of the Arab Formation in the studied field were mainly adopted from ADMA-OPCO, Abu Dhabi Marine Operating Company Study Team (1998).

GEOLOGICAL SETTING

The studied oilfield is situated in the offshore Abu Dhabi on the eastern part of the Arabian Platform, situated between two major structural highs, the Qatar Arch to the west and the Oman Mountains to the northeast (Figure 1a). This area has undergone relatively rapid subsidence since the Early Permian, resulting in the accumulation of a thick sedimentary section (Upper Permian to Recent section has a thickness exceeding 17,000 ft). The structural development of the area, which is typical of the Arabian Platform, is characterized by gentle simple folds, some of which are quite large. These folds are regarded as the expression of periodic reactivation of north-south aligned, deep-seated basement faults. In addition, salt tectonics has played an important role in the development and modification of structures in the area. The oilfield, which is part of this system, is an anticline with a flank dip of less than 5 degrees.

Organic geochemical analyses indicate that the peak oil generation and hydrocarbon charging occurred during the Eocene and that oil was sourced from the Jurassic source rocks of the Hanifa and Diyab formations.

The Arab Formation (Kimmeridgian) comprises four members labelled upward as Arab D, C, B and A. Arab D and C members, which are the main reservoirs, are the focus of this contribution (Figure 2a). The Arab B and A members comprise overall non-reservoir rocks. The Arab D is divided into four sub-zones (D5, D4, D3 and D2) and Arab C into three sub-zones (C3, C2 and C1). In offshore Abu Dhabi, the entire Arab Formation represents a regressive portion of a second-order supersequence, which is composed of four shallowing-upward third-order sequences. These sequences were deposited on a distally steepened ramp, characterized by an offshore break, owing to the presence of barrier islands and a slope. The occurrence of clinoforms in distal facies and the considerable spatial thickness variation in the Arab D4 and D3 between the ramp crest and the outer ramp suggest a distally steepened rather than homoclinal ramp. The Arab Formation is overlain by the Hith Formation (anhydrites and associated dolostones), which is the main seal in the area.

The Arab D and C members (≥ 700 ft thick) display considerable lateral and vertical facies variations depending on the location within the ramp (Figure 2b). The inner ramp comprises supratidal algal laminated mudstone/evaporite and lagoonal evaporite, wackestones, and packstones. The ramp crest comprises high-energy deposits of foraminiferal packstones, grainstones, floatstones, and intraclastic rudstones. The slope and outer ramps are composed of open-marine bioturbated wackestones and mudstones, with sponge spicules and relatively deep-water foraminifera (Figure 3). These deposits grade upwards into supratidal and shallow lagoonal evaporites of the Arab B and A members and the overlying Hith Formation. Thus, deposition in the inner ramp environments resulted in regressive cycles, which included shoal, lagoonal subtidal, and supratidal sediments. The amounts of evaporite

deposits increase upwards in the formation owing to the overall increasingly isolated to semi-isolated lagoon in relation to the open-marine environment of the outer ramp and ends with deposition of the evaporitic sulfate-dominated Arab B and A members. The lithology and distribution patterns of the inner-ramp deposits of the Arab Formation were greatly controlled by fluctuations in the relative sea level and paleo-climatic conditions.

LITHOLOGY

The lithology of Arab D and C includes sulfates, limestones and dolostones. Interpretation of the depositional facies was based on sedimentary structures and texture of the rocks.

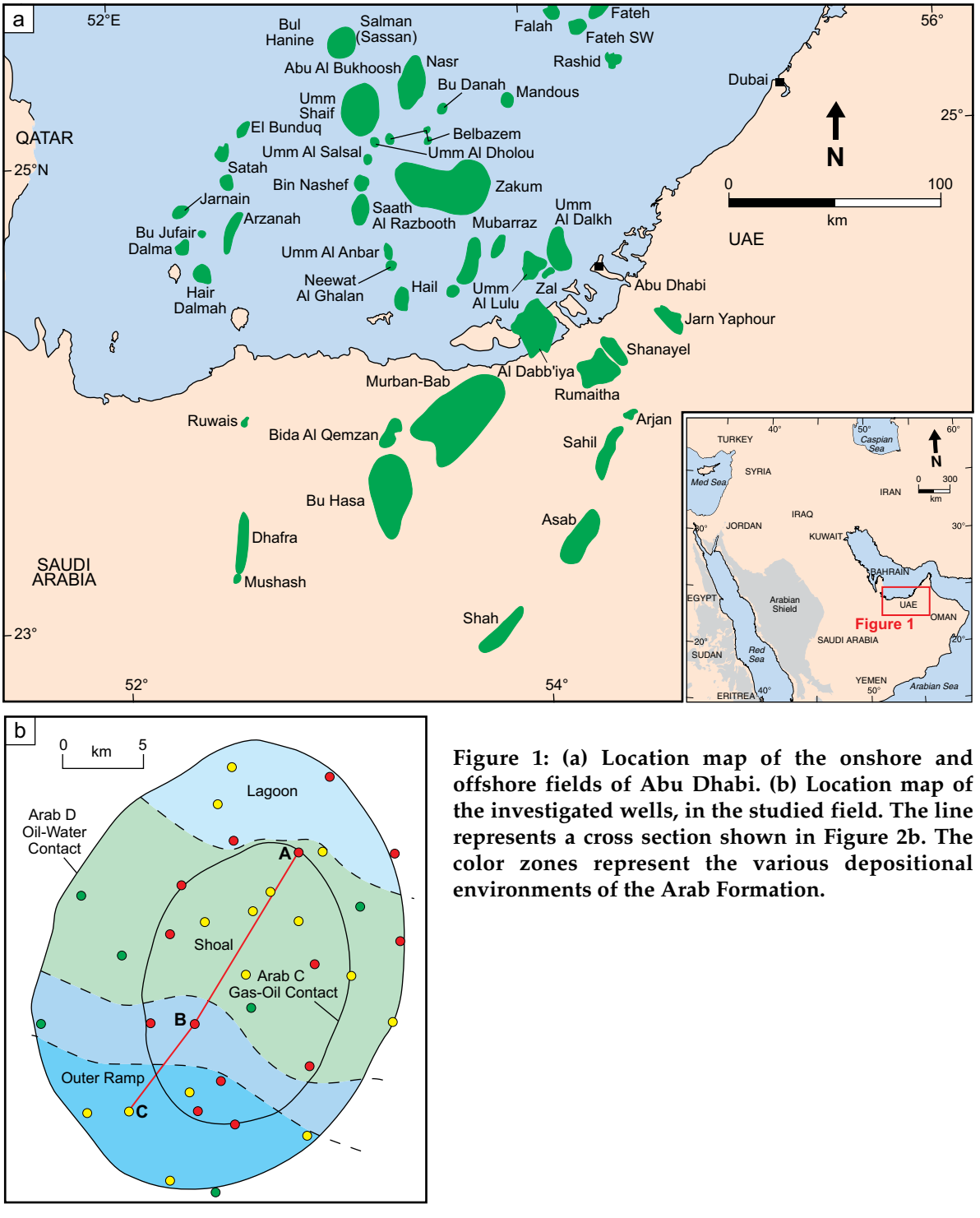

Figure 1: (a) Location map of the onshore and offshore fields of Abu Dhabi. (b) Location map of the investigated wells, in the studied field. The line represents a cross section shown in Figure 2b. The color zones represent the various depositional environments of the Arab Formation.

Sulfate Deposits

Two main occurrence patterns are displayed by the sulfate deposits, including:

1. Sulfate patches and nodules (1–10 cm across), which include mosaic, bedded mosaic, nodular mosaic, and nodular varieties (Maiklem et al., 1969), are coalesced, irregular in shape, and separated by a thin film of, or float in, dolomitic mud, are most common in Arab D2 and Arab C3, C2 to C1. The nodules, which are composed of parallel to sub-parallel lath-like and felted crystals (ca. 200–950 µm long) of anhydrite and subordinate gypsum, have commonly stylolitic contacts with the dolomitic mud. Nodular anhydrite is encountered in all wells except one, which comprises outer ramp deposits.

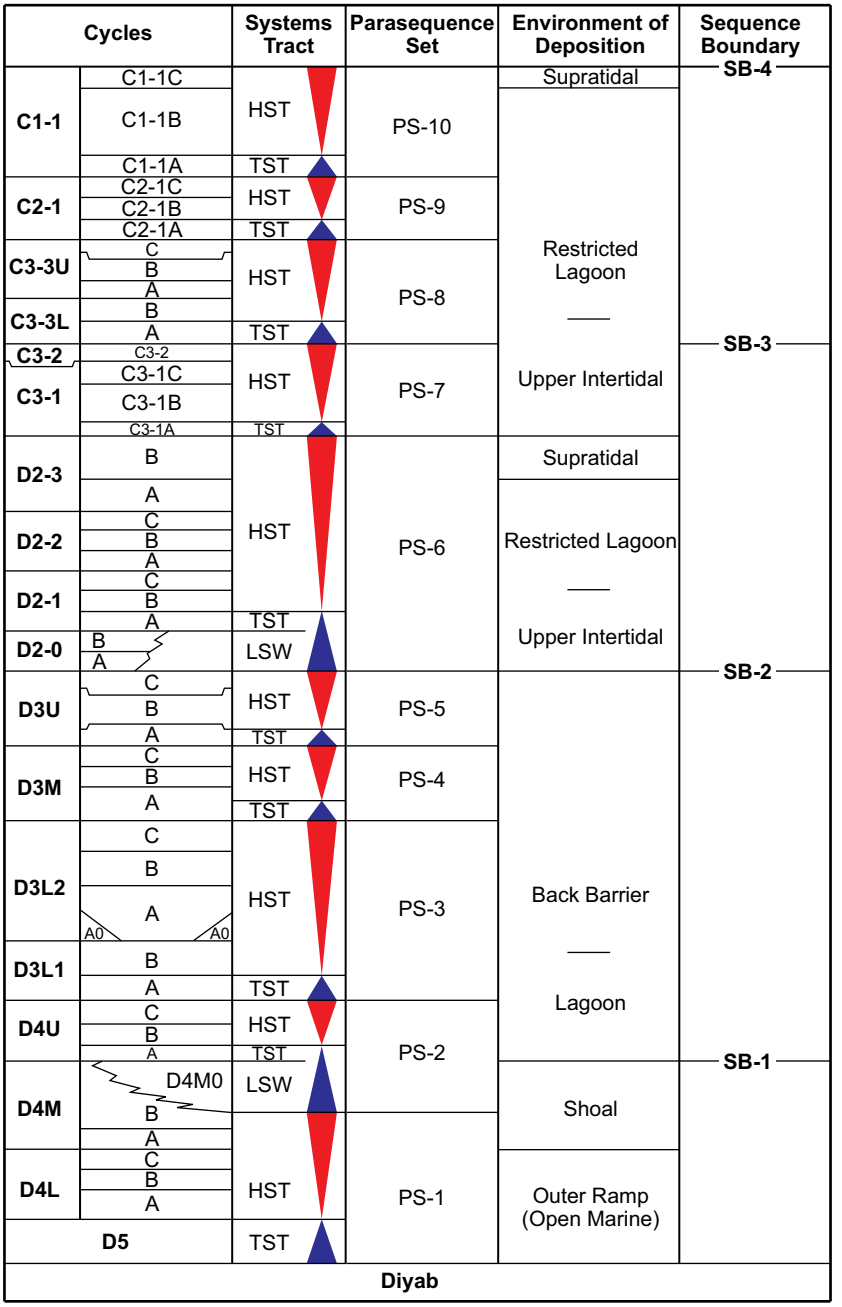

Figure 2: (a) Generalized sequence-stratigraphic column of the D and C members of the Arab Formation in the studied field.

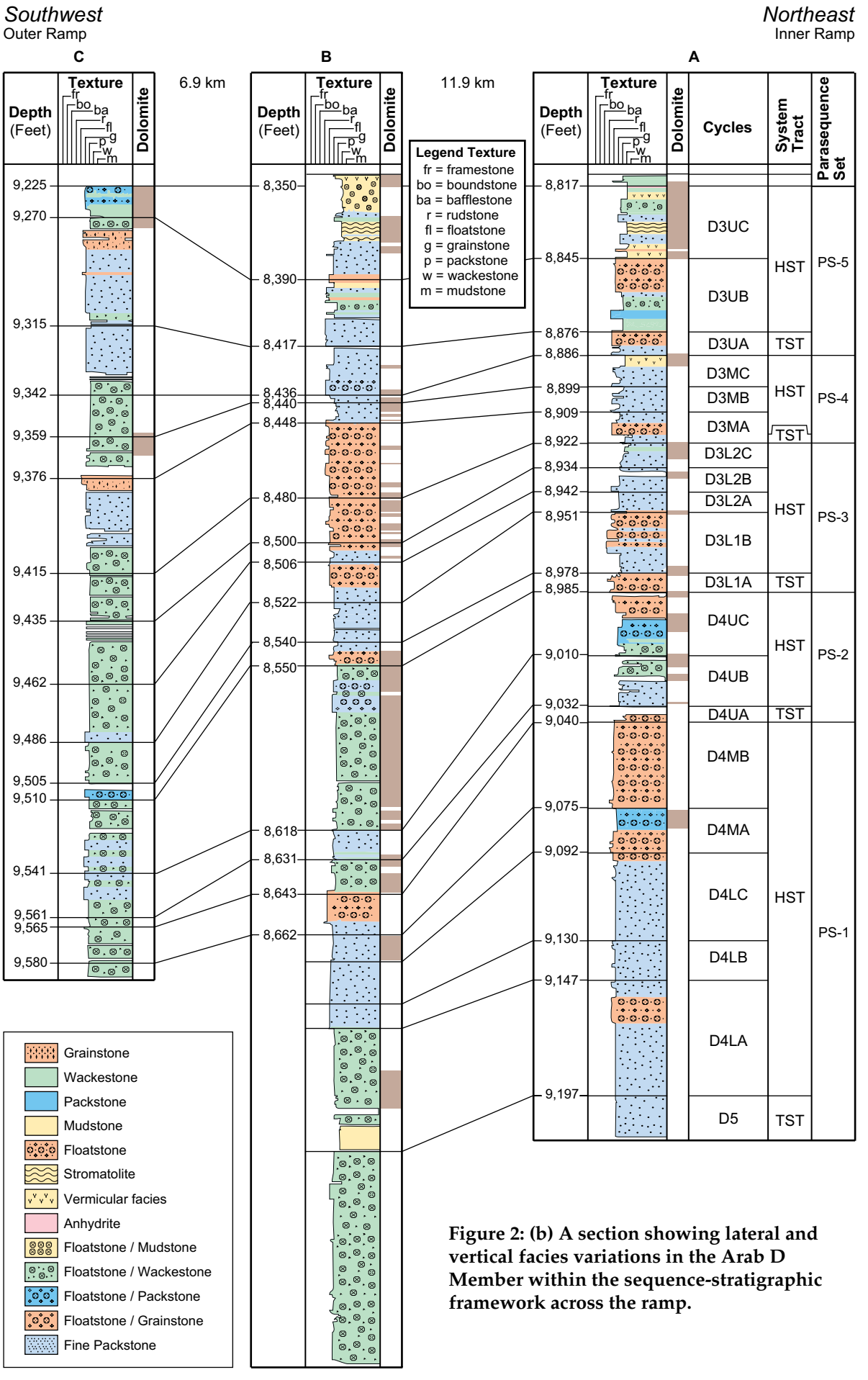

Figure 2: (b) A section showing lateral and vertical facies variations in the Arab D Member within the sequence-stratigraphic framework across the ramp.

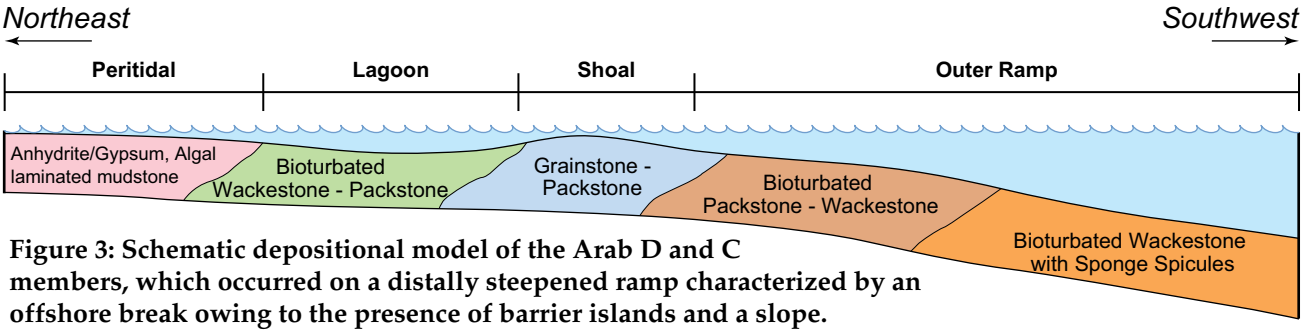

Figure 3: Schematic depositional model of the Arab D and C members, which occurred on a distally steepened ramp characterized by an offshore break owing to the presence of barrier islands and a slope.

2. Massive sulfate, which is less common than sulfate nodules, occurs as thin beds (0.5 to 1.5 ft) composed of coarse-crystalline, felted and acicular anhydrite and small amounts of gypsum. These sulfate beds occur in the Arab D2 and, less commonly, in the Arab C, with the lowermost stratigraphic occurrence being the base of the Arab D4 in a well to the northeast. Massive sulfates have been presumably precipitated subtidally in the lagoon during episodes of considerable fall in the relative sea level, which resulted in semi- and complete isolation of the lagoon from the open sea, i.e. in hypersaline lakes and ephemeral ponds, respectively (Warren, 2000).

The sulfate deposits are interpreted, based on occurrence habits, distribution pattern, sedimentary structures, and sulfur isotopes, to have been formed primarily in very shallow hypersaline lagoons (Azer and Peebles, 1995).

Limestones

Various types of limestones are recognized mainly in the Arab D5, D4 and D3, whereas their dolostone counterparts occur mainly in the Arab D2 and C. The limestone types encountered include:

Mudstones: These limestones, which are the least common, are algal laminated and interbedded with and have similar sedimentary structures as their dolostone equivalents in the Arab D2 and C. The limestones are interpreted to have been deposited in supratidal to upper intertidal environments bordering a shallow inner ramp and/or lagoon. Lime mudstones in the Arab D5, D4 and D3 are massive, non-algal laminated and are suggested to have been deposited in deeper-water environments of the outer ramp. This interpretation is suggested by the presence of planktonic foraminifera and the benthonic foraminiferid *Alveosepta* sp.

Wackestones: These are among the most common limestones in the Arab D and C, particularly in the southwestern part of the field, where bioturbated wackestones of the Arab D5 to D3 with sponge spicules indicate outer ramp (i.e. open-marine conditions). Lime wackestones in D2 and C1 are interpreted to have been deposited in a transitional shallow subtidal to upper intertidal environment, although with most deposition occurring subaqueously in a low-energy, semi-restricted lagoonal environment. Subtidal deposition is suggested by the occurrence of pelecypods, echinoids, and stromatoporoids, while restriction is indicated by the appearance of miliolids and dasyclad algae. Local intense bioturbation supports subaqueous conditions. The lime wackestones are gradational into lime mudstones and lime packstones with grains dominated by peloids and bioclasts.

Packstones: These limestones occur as 0.3 ft to ca. 3.3 ft thick beds, which are bioturbated, stylolitized and have scoured contacts, occur in the Arab D2 and C1 as interbeds with other limestones, dolostones and anhydrite. In the Arab D5 to D3, these limestones are massively interbedded with grainstones and wackestones. The grains in the packstones are dominated by peloids and bioclasts. Packstone deposition is interpreted to have occurred in shallow-water marine subtidal environments on a moderate-energy carbonate ramp ranging from outer-lagoon to outer-ramp environments.

Grainstones: Grainstones occur mainly in the Arab D4 and D3, where they commonly fine upwards into massively interbedded, bioturbated peloidal lime packstones and bioclastic lime wackestones (Arab D4) or with bioclastic intraclastic rudstones (Arab D3). The limestones occur sporadically in

the Arab D2 and C1 as thin (< 3 ft) dominantly bioclastic peloidal grainstones. The grains in the packstones are dominated by peloids and bioclasts (benthic foraminifera, calcareous algae, echinoids, pelecypods, and rare stromatoporoids) with rare to common, poorly-developed ooids and intraclasts. The grainstones are interpreted to have been deposited within beach-barrier island complex or shoals, which were developed seaward of the semi-restricted lagoon. The barriers were probably discontinuous with tidal inlets cutting through them perpendicular to the direction of the coastline and allowing variable extents (depending on the relative sea level), yet overall limited, circulation of seawater between the back-barrier lagoon and the open shelf. The discontinuous nature of the barriers explains the lateral facies variations encountered in the grainstone-rudstone packages of the Arab D4 and D3. The thin grainstones in the Arab D2 and C1 were probably deposited as spillover lobes, which extended from the barrier into the lagoon, or as low-amplitude sandwaves in the lagoon. Periodic emergence of the grainstones is suggested by the presence of desiccated bed contacts, fitted grain textures, and gypsum pseudomorphs.

Rudstones: These limestones occur as bioclastic intraclastic rudstones interbedded with coarse-grained grainstones mainly in the Arab D4 and D3 and sporadically in Arab D2. Deposition is inferred to have occurred in a high-energy upper shoreface to foreshore environment associated with beach-barrier island complexes. The high degree of grain rounding suggests prolonged reworking by waves, while development of decimeter-thick shallowing-upwards cycles suggests repeated progradation over lower shoreface grainstones. The rudstones are laterally discontinuous and form prograding clinoforms or ramp-margin wedges (RMW) or lowstand wedges (LSW).

Dolostones

The Arab Formation dolostones display textural and structural features, which provide clues to the origin of parent rocks, including:

1. **Dolomudstones and dolowackestones:** These dolostones, which are formed by dolomitization of mudstones and wackestones, are buff-colored, oil-stained, scoured, bioturbated (mostly bored), and algal-laminated, and occur in the Arab D2 and Arab C and sporadically in the Arab D4 and D3, being closely associated with sulfate beds. These dolostones may act as baffles/barriers to vertical fluid flow owing to their low permeability. Fenestral vugs (birds-eye structures), which are filled by coarse crystalline anhydrite with subordinate gypsum and microcrystalline dolomite rhombs, are common.
2. **Dolopackstones and dolograinstones:** These dolostones are more common in the Arab D2 and C than in the Arab D5 to D3. In the Arab D2 and C, these dolostones show planar and, less commonly, low-angle cross- and ripple lamination, bioturbation and stylolitization. The dolostones occur within 10–25 ft thick, progradational packages (parasequences) with wackestones at the base, passing upwards into interbedded bioclastic peloidal dolopackstones and dolograinstones capped by nodular anhydrite. In the Arab D5 to D3, these dolostones are interbedded with their corresponding limestones and display stylolites and sparse sedimentary structures, presumably due to extensive bioturbation. Grains in the dolostones include very fine- to medium-grained peloids, pelecypods, dasyclad algae, echinoids, benthic foraminifera, and rare ooids. Sand- to pebble-sized, rounded to sub-rounded micritic intraclasts occur locally.
3. **Dolorudstones and dolofloatstones:** These dolostones are the least common being encountered in the Arab D3 of a well located to the south and in the Arab D4 of a well to the east (Figure 1b). These dolostones are rich in large moldic pores.
4. **Undifferentiated dolostones:** These are the most common types of dolostones, being most common in the Arab D2 and C. The dolostones occur as decimeter thick interbeds with sulfates, other types of dolostones, and rare limestones. These dolostones lack recognizable grain types and sedimentary structures, which makes it difficult to recognize the precursor limestones or their depositional environments. However, the commonly coarse-crystalline texture of dolomite crystals and their presence within sand-sized, vaguely defined moldic pores suggests that these dolostones have lime grainstone precursors, whereas the fine-crystalline dolostones that are associated with sulfate deposits are likely to be dolomitized peritidal mudstones.

SEQUENCE STRATIGRAPHY AND RELATED LITHOFACIES

The sequence-stratigraphic framework of Arab D and C is adapted mostly from De Matos and Hustrand (1995), a confidential report prepared by ADMA-OPCO Team (1998), and papers published by Al-Suwaidi and Aziz (1998, 2002). These authors interpreted the entire Arab Formation as a second-order regressive segment supersequence consisting in the Arab D and C of three third-order sequences. The supersequence is composed of a four-fold hierarchy ranging from sequences to cycles, which have been interpreted to correspond to transgressive-regressive episodes driven by low-amplitude fluctuations in global sea level (i.e. eustasy; Azer and Peebles, 1998). The sequence-stratigraphic framework of Arab D and C is that of a distally steepened ramp characterized by thick regressive events or highstand systems tracts (HST) and thin transgressive systems tracts (TST). Four unconformity-bounded sequences (0.5 to 5 million years) have been recognized (Al-Suwaidi and Aziz, 1998, 2002).

Deposition of the first sequence commenced by the formation of a thick TST of the Arab D5 limestones, which are bounded at the top by a maximum flooding surface (MFS), followed by the deposition of a HST associated with progressive shallowing upwards (Figure 2). Four sequence boundaries (SB) are distinguished in the Arab D and C, encompassing three sequences. A type-1 SB at the top of this HST occurs at an erosional surface on top of the Arab D4M. A lowstand wedge (LSW) named D4M0 was deposited over D4M in the southeast of the ramp (Figures 2a and 2b). The presence of LSW to the southwestern part of the ramp above the Arab D3UC (called D2-0) suggests that the top of D3U is possibly a type-2 SB. This SB represents an amalgamated surface of subaerial exposure and subsequent transgression (i.e. transgressive surface TS), which is evidenced by the presence of bored firmground with an intraclastic lag. The third SB occurs on top of the Arab C3-2 as a surface below which the sediments display abundant moldic pores and vugs. A fourth SB is put at the top of the anhydrite, which caps the Arab C reservoir, called C1-1C in this paper. De Matos and Hulstrand (1995) have recognized two similar surfaces of subaerial exposure within the Arab D and C in the southeastern onshore fields. Whether SB-3 and SB-4 are of type-1 or type-2 is not fully understood (Al-Suwaidi and Aziz, 2002). The latter authors have therefore suggested the presence of three third-order sequences. The anhydrite beds are considered here to represent deposition as part of late HSTs denoting fall in the relative sea level (i.e. regressive), capping sequences, parasequence sets, or cycles. Based on the sequence-stratigraphic framework, the Arab D and C in Central Saudi Arabia have been interpreted to represent two depositional sequences with the anhydrite caps (Le Nindre et al., 1990). De Matos and Hulstrand (1995) recognized two main depositional sequences within the Oxfordian and Kimmeridgian successions of onshore and offshore Abu Dhabi.

Parasequence Sets

The three sequences, which are bounded by sequence boundaries (SB), in the Arab D and C are subdivided into ten shallowing upward parasequence sets (PS; Figures 2a and 2b). These PSs display distinctive log patterns or motifs, which greatly aid their field-wide correlation. However, correlation of successions to the southwest of the field, which were deposited in open-marine environments, is more problematic because cyclicity is pronounced. Each PS starts with a deepening component composed of a thin TST at the base capped by a MFS/condensed section (CS), which is overlain by a shallowing component (HST) (cf. Azer and Peebles, 1998). The TST shows relatively deeper facies (subtidal-lower intertidal) characterized by horizontal to low-angle laminations, bioturbation, mottling, intraclasts, discrete anhydrite/gypsum nodules and gypsum rosettes (Azer and Peebles, 1998). The TST is generally composed of low-permeability, bioturbated lime mudstones/wackestones capped by a bored and burrowed firmground, which constitutes the marine (or maximum) flooding surface (i.e. condensed section).

Azer and Peebles (1998) concluded that the MFS/CS is characterized by laterally extensive (10s of kilometers), thin, discontinuous, lensoid-bodied anhydrite, which has been formed by replacement of gypsum deposited in salt basins. The HST comprises grainstones and packstones with good porosity and permeability. These grain- and packstones are commonly capped by low-permeability

lime mudstones, which are deposited during the next marine flooding event. The Arab D5 to D2 succession comprises six PSs, which are capped by dense, low permeability lime or dolomudstones, commonly showing fenestral pores filled with dolomite and/or anhydrite. The Arab C comprises four PSs, which are capped by anhydrite (cf. Azer and Peebles, 1998). PS-1, which includes the D5 to D4M (up to 240 ft thick), is progradational, PS-2 to PS-5 (D4U to D3U) are interpreted to be retrogradational (fining upwards), and PSs of the Arab D2 and C are interpreted to be progradational, and are commonly capped by anhydrite. Typical features of the HST include the presence of intraclasts (in lag grainstones or rudstones), mollusks, ripple lamination, scour surfaces, algal lamination, and, in some cases, erosional surfaces (Azer and Peebles, 1998).

Parasequences

Parasequences (or cycles), which are either episodic or periodic, occur in retrogradational, aggradational, and progradational PSs. The parasequences are always progradational. Episodic cycles (Arab D5 to D3) have limited spatial distribution and short duration, whereas periodic cycles (Arab D2 to C) have great spatial distribution and systematic changes in thickness. The distinction of parasequences in the Arab D5 to D4M, which do not represent typical cycles, is made based on petrophysical characteristics. Apart from the pinch outs of LSW, the Arab D and C are subdivided into 28 and 15 parasequences (cycles), respectively. Parasequences in the Arab D5 to D3 ranges in thickness from 5 to 70 ft, whereas in the Arab D2 and C, cycle thickness ranges from 2 to 20 ft.

An ideal cycle in the Arab C is composed of five components, in an upward direction: (a) transgressive lag with intraclastic pebbles (< 1 ft thick) formed by marine erosion sediments; (b) TST peloidal dolopackstones with patchy anhydrite cement; (c) dolomudstones to dolowackestones along condensed section (marine flooding surface; < 1 ft thick); (d) early HST dolowackestones (shallow subtidal to upper intertidal, low-energy lagoon); and (e) late HST anhydrite (subtidal to supratidal). Cycles in the LSW of D2 consist of partly dolomitized packstones/grainstones (containing molluscs, peloids, and stromatoporoids) and intraclastic rudstones/floatstones with good porosity-permeability. These cycles are bounded by hardground and erosive contacts. In the section deposited in open-marine environment, the cycles are composed of bioclastic floatstones, which display gradual dolomitization upwards towards the marine flooding surface.

The cycles in sub-zones D2-1 of the inner ramp and restricted lagoon begin at the base with: (a) peloidal dolopackstones/dolowackestones, overlain by dolomudstones/dolowackestones with fenestral pores and capped by surface of subaerial exposure; (b) peloidal grainstones capped with floatstones with a scoured dolomitized surface; and (c) peloidal grainstones with abundant moldic porosity, capped by a hardground. The overlying cycles of sub-zone D2-2 are composed of algal-laminated dolomudstones with fenestral pores capped by thin anhydrite or thin dolopackstones and firmgrounds. The overlying D2-3A is composed of bioturbated dolomudstones/dolowackestones, whereas cycle D2-3B is made of variable types of anhydrite. The typical lithological and petrological ordering of parasequences of the Arab Formation varies spatially across Abu Dhabi (Azer and Peebles, 1998).

Cycles in the Arab D5 to D3 thicken from the inner to ramp crest and thin again in the outer ramp. The cycles in the Arab D5 to top D4M begin with wackestones, packstones are finally capped by grainstones. Above sub-zone D4M, a LSW cycle (D4M0) occurs in the southeast and consists of pebble-sized, intraclastic, stromatoporoidal rudstones. The overlying cycles of D4U, which are associated with marine flooding, include D4UA, which consists of lime mudstones at the base grading to peloidal packstones/wackestones and capped by bioturbated lime mudstone. Successive shallowing upward cycles consist of bioclastic, intraclastic wackestones/packstones capped by grainstones (rich in moldic pores) and thin mudstones. Laterally, the D4U cycles change gradually in the southwest part of the field (outer ramp) to highly stylolitized wackestones and packstones rich in echinoderm, sponge spicules, and ostracodes. The upper cycle (D4UC) of D4U at the platform margin consists of dolowackestones.

The Arab D3L cycles are composed of peloidal, stromatoporoidal packstones/grainstones overlain by tidal flat cycles composed of peloidal packstones and bioturbated, algal laminated mudstones. Over the platform, cycles of D3L are commonly grain-dominated. Cyclicity is not distinct in the outer ramp in which the sediments consist of bioturbated spiculitic, highly stylolitized, and probably highly fractured, bioclastic wackestones. The Arab D3M is divided into three cycles, which are in ascending order sub-zones D3MA, D3MB, and D3MC. The D3MA cycle is dominated by packstones and grainstones bounded by erosional surfaces. The overlying D3MB and D3MC cycles are composed of bioturbated packstones and grainstones with occasional firmgrounds and are capped by dolomudstones with erosive and stylolitic upper contacts. In the outer ramp, these cycles are bioclastic (in some cases spiculitic), dolomitic wackestones and packstones, which may contain large silica nodules and stylolites.

The Arab D3U is divided into three cycles (a) sub-zone D3UA is composed of coarse-grained lag of stromatoporoids peloid grainstones/packstones with an upper stylolitic hardground, (b) sub-zone D3UB consists of wackestones and grading upwards into peloidal, intraclastic packstones/grainstones, and (c) sub-zone D3UC consists of a fining upward, peloidal dolopackstones and dolowackestones, and finally dolomudstones with fenestral pores, which are capped by an anhydrite bed. The D3U in the outer ramp to the southwest consists of dolopackstones and dolomudstones with anhydrite cement, silica nodules, and stylolites. At the platform margin, Arab D3U cycles consist of lime grainstones, which are dolomitized in the upper parts.

The lateral and vertical facies variations in the Arab D and C members within the sequence-stratigraphic framework across the ramp are outlined in Figure 2b.

BURIAL-THERMAL HISTORY OF THE BASIN

The burial history of the study area is typical for foreland basins including progressive burial. However, an event of significant decrease in isothermal gradient during Late Cretaceous is attributed to uplift caused by the obduction of Oman ophiolites (Figure 4). The rate of subsidence has increased episodically yet at relatively regular intervals of ca. 20 million years. The top Arab configuration during the Early Cretaceous (Aptian) suggests that the oilfield structure was already a four-way dip closure with a vertical relief of ca. 250 ft. Active structural growth occurred throughout the Late Cretaceous and Tertiary and led to formation of the present-day structure of the field with a vertical closure of ca. 1,400 ft. Organic geochemical analyses indicate that oil maturation in the source rocks (Jurassic Diyab Formation) started around mid Cretaceous, but peak oil generation and migration into Jurassic reservoir rocks of the Arab Formation occurred during the Eocene.

Samples and analytical methods

This study is based on petrographic examination of nearly one thousand thin sections from 16 selected wells (Figure 1b). These wells cover the entire field, including the crest and flanks of its anticlinal structure. Four hundred and ninety-six representative core samples have been selected from these wells along the structure covering the various encountered depositional settings (i.e. supratidal, lagoon, inner ramp, shoal, and outer ramp). Detailed petrographic, geochemical, and fluid inclusion analyses were conducted on these samples.

The chemical compositions of carbonates were determined on carbon-coated thin sections using a Cameca BX50 electron microprobe (EMP) equipped with three spectrometers and a back scattered electron (BSE) detector. The operations conditions include 10 KV acceleration voltages, 5–10 nA measured beam current, and defocused beam unless the crystal size or area to be analyzed was too small. The standards and count times used were natural wollastonite (Ca, 20 seconds), synthetic MgO (Mg, 80 s), $MnTiO_3$ (Mn, 80 s), hematite (Fe, 60s), and strontianite (Sr, 80 s). The EMP detection limits for trace elements were ca. 100 ppm; analyses within two standard deviations of the background were assumed to be below detection limit.

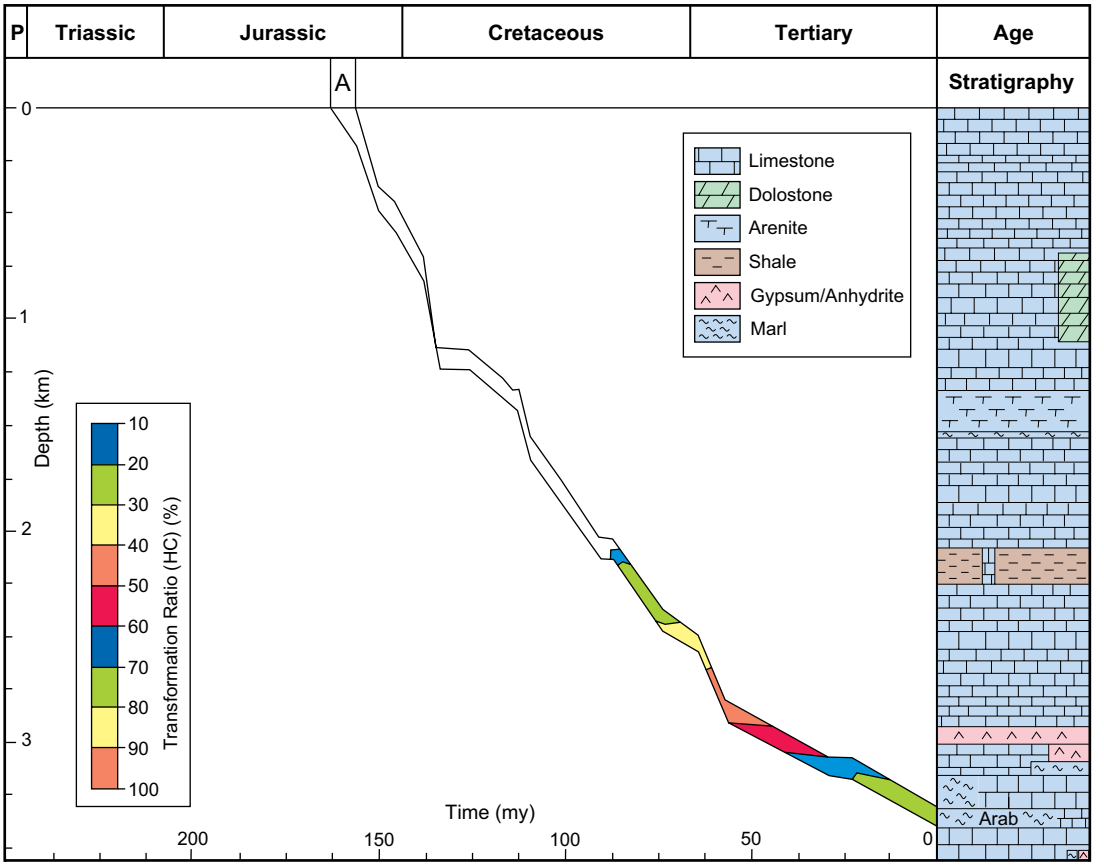

Figure 4: Burial-thermal history curve of the studied basin. Note the decrease in the isothermal line in Late Cretaceous, which was presumably caused by uplift during the obduction of Oman ophiolites.

A dental drill mounted on a microscope was used to micro-sample the different carbonate phases to be analyzed for oxygen, carbon and strontium isotopes. The oxygen and carbon isotope analyses (n = 172) were performed on the obtained carbonate. The powders were reacted in vacuum with 100% pure phosphoric acid for four hours at 25°C. For mixed calcite-dolomite samples, analyses were made on samples obtained using the chemical separation method of Al-Aasm et al. (1990). The evolved CO_2 gas was analyzed for isotopic ratios on a Delta-plus mass spectrometer. The phosphoric acid fractionation factor used was 1.01025 for calcite (Friedman and O'Neil, 1977). The precision of carbon and oxygen isotope values are better than 0.05‰. The isotopic data are presented in the normal δ notation relative to V-PDB. The ratio of $^{87}Sr/^{86}Sr$ isotopes were obtained (n = 118 samples) using an automated Finnigan 261 mass spectrometer equipped with nine Faraday collectors. Correction for isotopic fractionation during the analyses was made by normalization to $^{86}Sr/^{88}Sr = 0.1194$. The mean standard error of mass spectrometer performance was ± 0.00003 for standard NBS-987.

The micro-thermometric measurements were performed using a Linkam THMS600G heating-freezing stage. Petrography of fluid inclusions (FIs) was studied on the selected unheated and unstained wafers using a petrographic microscope equipped with ultraviolet epi-illumination. Special emphasis was placed on primary fluid inclusions, which were distinguished in fluid inclusions assemblages (FIA), i.e. petrographically associated groups of inclusions, presumably trapped at about the same time (Goldstein and Reynolds, 1994). A total of 600 micro-thermometric measurements were performed on primary aqueous and oil inclusions. The instrument thermocouple was calibrated using synthetic pure-water and CO_2 inclusions. Homogenization temperatures (T_h) were measured first before final ice melting temperatures (Tm_{ice}) in order of increasing temperature to avoid FI overheating (Goldstein and Reynolds, 1994). The salinity of aqueous fluid inclusions, expressed as weight per cent of NaCl equivalent, was calculated from Tm_{ice} using the Bodnar (1992) equation. It should be noted that the T_h measurements represent the lowest possible entrapment temperatures.

PETROGRAPHY

Limestones

The main diagenetic features in the limestones (particularly packstones, grainstones and floatstones) include: (1) development of micrite envelope (5–10 μm wide) around the allochems; (2) calcite cementation; (3) dolomite cementation and replacement; (4) recrystallization; (5) dissolution; (6) anhydrite/gypsum cementation; and (7) other minor cement precipitation (e.g. pyrite, fluorite and quartz).

Isopachous rim calcite (referred to here as C1) around the allochems mostly occur in the TST and HST of the Arab D3 unit. The calcite rims are composed of scalenohedral (dogtooth like) to prismatic crystals, with main growth axes perpendicular to the grain surfaces and vary in length from about 10 μm to 180 μm (Figures 5a and 5b). Equant calcite crystals (mostly 20–150 μm across; referred to here as C3), which fill intergranular, intragranular and moldic pores, occur mostly in LSW and HST of the Arab D4 and D3 cycles. Intragranular and moldic pores were formed by dissolution of aragonitic allochems. Equant calcite engulfs, and thus post-dates the isopachous calcite rim (Figure 5c). Syntaxial calcite overgrowths (referred to here as C2), up to 450 μm thick, developed around crinoids, filling the adjacent intergranular pore spaces. The overgrowths engulf isopachous calcite rims and are engulfed by equant calcite and dolomite (Figure 5d). When growing into large intergranular pores, the calcite overgrowths display euhedral crystal faces. In some cases, the overgrowths fill intragranular/moldic pores, which have resulted from dissolution of peloids. Grainstones containing scattered patches of syntaxial calcite overgrowths and equant calcite are commonly characterized by high intergranular porosity (Figure 5d).

The grainstones and packstones are commonly cemented by scattered dolomite crystals (ca. 50–800 μm across), which fill inter- and intragranular pores (Figure 5e); dolomite has also partly replaced the grains and matrix. Partial dolomitization is commonly accompanied by slight to severe dissolution of the peloids and micrite matrix. The dolomite crystals are subhedral (planar-s) to euhedral (planar-e; Sibley and Gregg, 1987). In a few limestones, dolomite cement has extensively filled the intergranular pores (Figure 5f). Less commonly, dolomite cement occurs as finer crystalline (mostly 10–50 μm), interlocked rhombic crystals, which fill intergranular and secondary intragranular/moldic pores (resulted from allochem dissolution; Figure 5g). Dolomitization of wackestones is in some cases localized to zones a few mm to a few cm across, which are presumably sites of bioturbation. Coarse dolomite rhombs engulf and replace (partly to completely) the syntaxial calcite overgrowths. Upon complete replacement, the dolomite appears as overgrowths around non-dolomitized crinoid grains (Figure 5h).

The grainstones, rudstones, and packstones contain variable amounts of intragranular and moldic pores, which have resulted from partial to complete dissolution of peloids and bioclasts (Figure 6). Moldic pores are most abundant in grainstones and rudstones of the LSW. These grainstones and rudstones are commonly cemented by equant calcite (Figure 6b) and are thus often poorly connected with each other and with the overall pore system in these limestones. Apart from rare, partial dissolution of the isopachous calcite rim in some of the grainstones, there is no evidence of significant cement dissolution in the limestones.

Anhydrite and gypsum are volumetrically insignificant in most of the limestones. These minerals occur as scattered blocky crystals (up to 800 μm across), which fill the intergranular pores, partly to completely replace the grains and calcite cements, and engulf and partly replace rhombic dolomite cement in the grainstones crystals (Figures 7a–d). Sulfate minerals also occur in the wackestones where they replace the peloids and the micrite matrix. Cementation by these sulfates is most common in the vicinity of micro-fractures. Sulfate cement engulfs the isopachous calcite rim and syntaxial calcite overgrowths around the grains as well as the equant calcite and the dolomite.

Scattered framboidal pyrite and cubic crystals of fluorite (ca. 350–800 μm across) have replaced the micrite matrix and peloids in some of the limestones. The wackestones, which were deposited in the outer ramp, are locally replaced by chalcedony and microcrystalline quartz. The replacement is

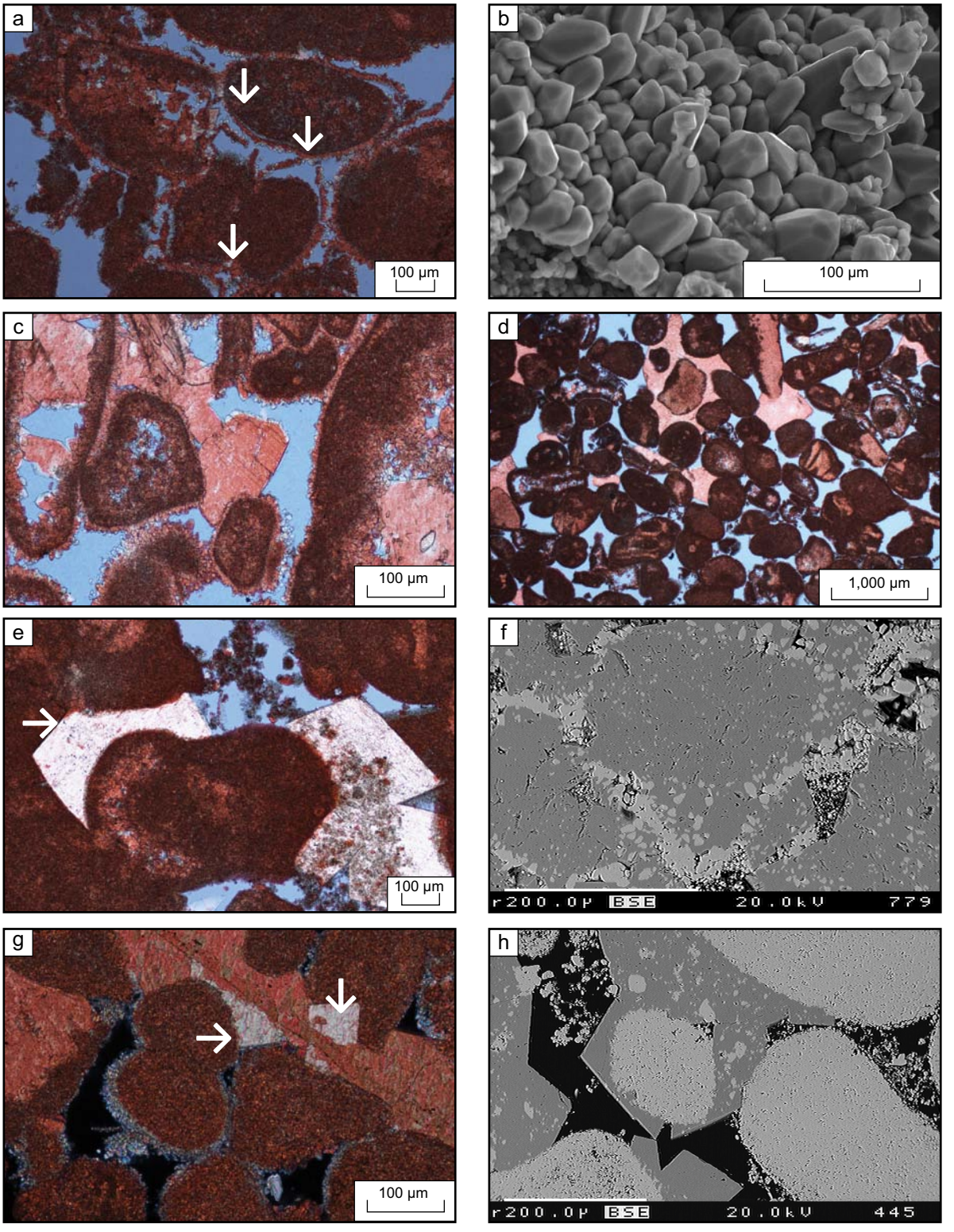

Figure 5: Isopachous, blocky/equant, syntaxial overgrowth calcite cements, and dolomite cements. (a) Optical photomicrograph (PPL, plane polarized light) showing spalled isopachous rims (arrows), which resulted in small pore space between the rim and the grain. (b) SEM image showing the isopachous rim in TST grainstones composed of small scalenohedral crystals with main growth axes perpendicular to the grain surface. (c) Optical photomicrograph (PPL) of inter- and intragranular equant calcite cement, which engulfs isopachous calcite rims around the grains. (d) Optical photomicrograph (PPL) showing a grainstone containing scattered syntaxial calcite overgrowths and equant calcite and high intergranular porosity. (e) Optical photomicrograph (PPL) showing dolomite cement that occurs as euheudral crystals that conform to pore shape (arrow). (f) Back-scattered electron image showing fine-crystalline dolomite (light grey) which fills moldic and intergranular pores and engulfs the preserved scalenohedral calcite rims and equant calcite cement. (g) Euhedral dolomite around peloid has been presumably formed by dolomitization of syntaxial calcite overgrowth; the calcitic grain itself was not subjected to dolomitization. (h) Backscattered electron image of dolomite rhombs which have replaced syntaxial calcite overgrowths.

either restricted to a few scattered peloids, or resulted in the formation of silica nodules (Figure 7d). Rarely, there are partly silicified, outer ramp mudstones that are rich in glauconite, which occurs as fine-crystalline flakes.

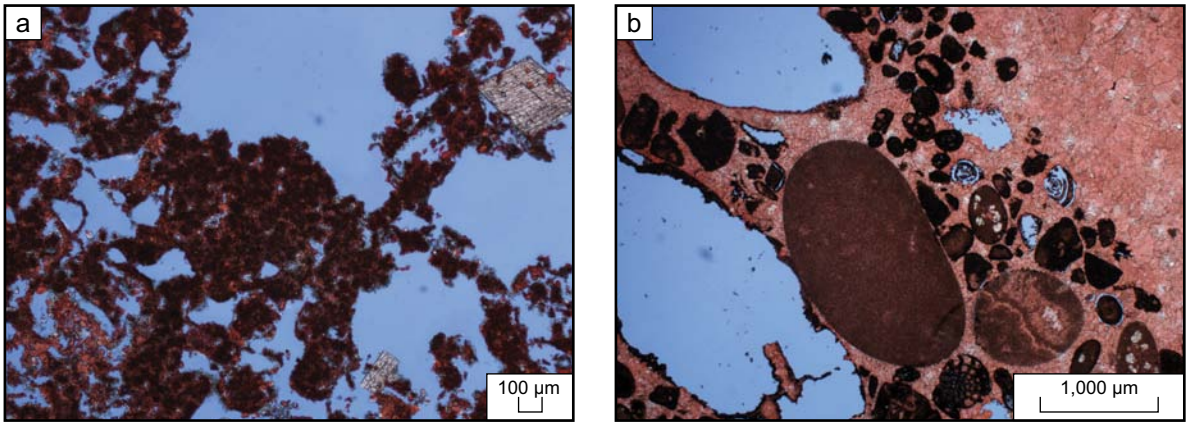

Figure 6: Optical photomicrographs (PPL) showing: (a) Grainstone in which the intragranular and moldic pores formed by grain dissolution are well connected to each other. Note the presence of scattered dolomite rhombs, which may help supporting such porous grainstones against compaction. (b) Rudstone in which the moldic pores are isolated from each other by extensive pore-filling equant calcite cement.

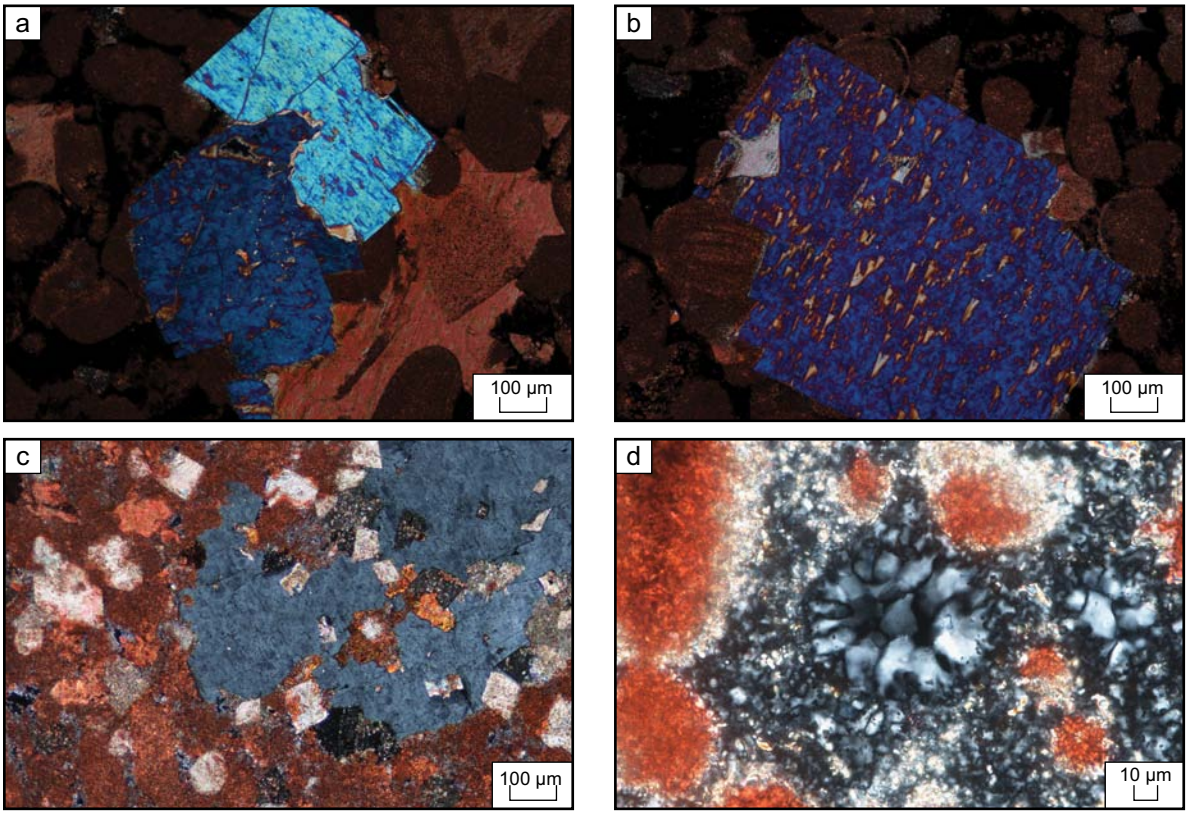

Figure 7: Optical photomicrographs (XPL) showing sulfate cement and silicification in the limestones; note that these sulfates replace lime grains, matrix and calcite cement. (a) Anhydrite crystals engulf and slightly replace syntaxial calcite overgrowths. (b) Large anhydrite crystal which has replaced several grains in a grainstone. (c) A large gypsum crystal, which has pervasively replaced the lime grains and engulf and partly replace dolomite crystals. (d) Part of a silica nodule in which the host wackestone is partly preserved.

In addition to the expected increase in sediment packing owing to increasing overburden pressure, there is ample evidence of grain deformation and pressure dissolution (i.e. mechanical and chemical compaction). The stylolites vary widely in lateral extent, amplitude (a few mm to a few cm) and commonly run parallel or nearly parallel to the bedding planes, though in some cases they deviate to run oblique to bedding. Tectonic compression of the limestones presumably accounts for the formation of vertical stylolites, which taper into and cross-cut, and thus post-date, horizontal stylolites. The stylolitic surfaces contain variable amounts of bitumen and, in some cases, scattered rhombs of dolomite. Empty micro-fractures occur within and in the vicinity of stylolites.

Dolostones

The main diagenetic features in the dolostones include: (1) various dolomitization textures; (2) anhydrite/gypsum cementation; (3) calcite cementation and dolomite calcitization; (4) dissolution and sulfate cementation; (5) quartz cementation; (6) minor cements; and (7) stylolitization.

The textural variations among the dolostones are strongly controlled by the type of parent limestone. Dolomitization of the peritidal mudstones has commonly resulted in the formation of micro-crystalline dolostones, which may or may not have preserved algal lamination (Figure 8a). Dolomitization of the grainstones is dominantly fabric destructive and has resulted in the formation of a fine- (5–10 μm); medium- (> 10–50 μm) to coarse-crystalline (> 50–150 μm across), mosaic of euhedral to subhedral dolomite (Figure 8b). Dolograinstones and dolorudstones contain variable amounts of moldic pores, possibly after dissolution of aragonitic bioclasts. The dolostones may contain large patches of tightly packed, anhedral dolomite, which possibly resulted from the dolomitization of mud intraclasts and/or peloids. Dolomitization of the grains and matrix is most extensive in the Arab D2 and C, particularly along the MFS. These dolostones are closely associated with gypsum and anhydrite cements. In addition to the replacive dolomite phase, dolomite cement fills intergranular pores being most common in extensively dolomitized grainstones. The dolomite cements may form rims (referred to here as DC3) around inclusion-rich, dolomite crystals (referred to here as DC2; Figure 8b). As is the case with all other carbonates cements in the Arab Formation, these euhedral dolomite crystals (Figure 8c) are non- to dull- luminescent.

Blocky to poikilotopic anhydrite and gypsum cements fill intercrystalline pores as well as intragranular and moldic pores in dolomudstones and dolograinstones of the Arab D2 and C (referred to here as AN2; Figures 8c–f). In most cases, these sulfate cements replace the dolomite crystals. These sulfate cements are far more common in the HST than in the TST. Fractures filled with gypsum and anhydrite cements (referred to here as AN3) are common in the dolostones. The fracture-related sulfate cements contain primary oil inclusions denoting precipitation during a phase of oil charging into the reservoir.

Calcite cement occurs also as coarse blocky crystals, which occupy intercrystalline pores in dolostones (Figures 9a and 9b). This calcite cement is closely associated with and, in relatively rare cases, partly replaces anhydrite cement. The intercrystalline calcite cement is not cross-cut by the stylolite planes, and thus may post-date stylolitization. This type of calcite cement occurs mainly in the Arab D2 and C.

Porosity in the dolostones has resulted from the dissolution of dolomite as well as of intercrystalline, moldic, and intracrystalline anhydrite/gypsum cements (Figures 9c and 9d). Dissolved sulfate cements (AN2) leave behind etched crystals and tiny remnants scattered throughout the dolostone. The dolostones contain intragranular and moldic pores, which have resulted from partial to complete dissolution of allochems (Figures 9e and 9f). Intercrystalline porosity, which has resulted from dolomitization of grainstones and packstones, is larger in size and better inter-connected than inter-crystalline porosity in dolomitized mudstones and wackestones.

Authigenic quartz lines the moldic pores, engulfs and replaces (i.e. post-dates) rhombic dolomite, and fills intragranular/moldic pores; quartz is engulfed by, and thus pre-dates, anhydrite cement (Figures 9g and 9h). The quartz crystals have hexagonal and, in some cases, rhombic crystal forms. Microcrystalline quartz fills moldic pores together with extensively dissolved anhydrite cement. This type of quartz cement occurs as rounded, inclusion-rich bodies, which are surrounded by a layer

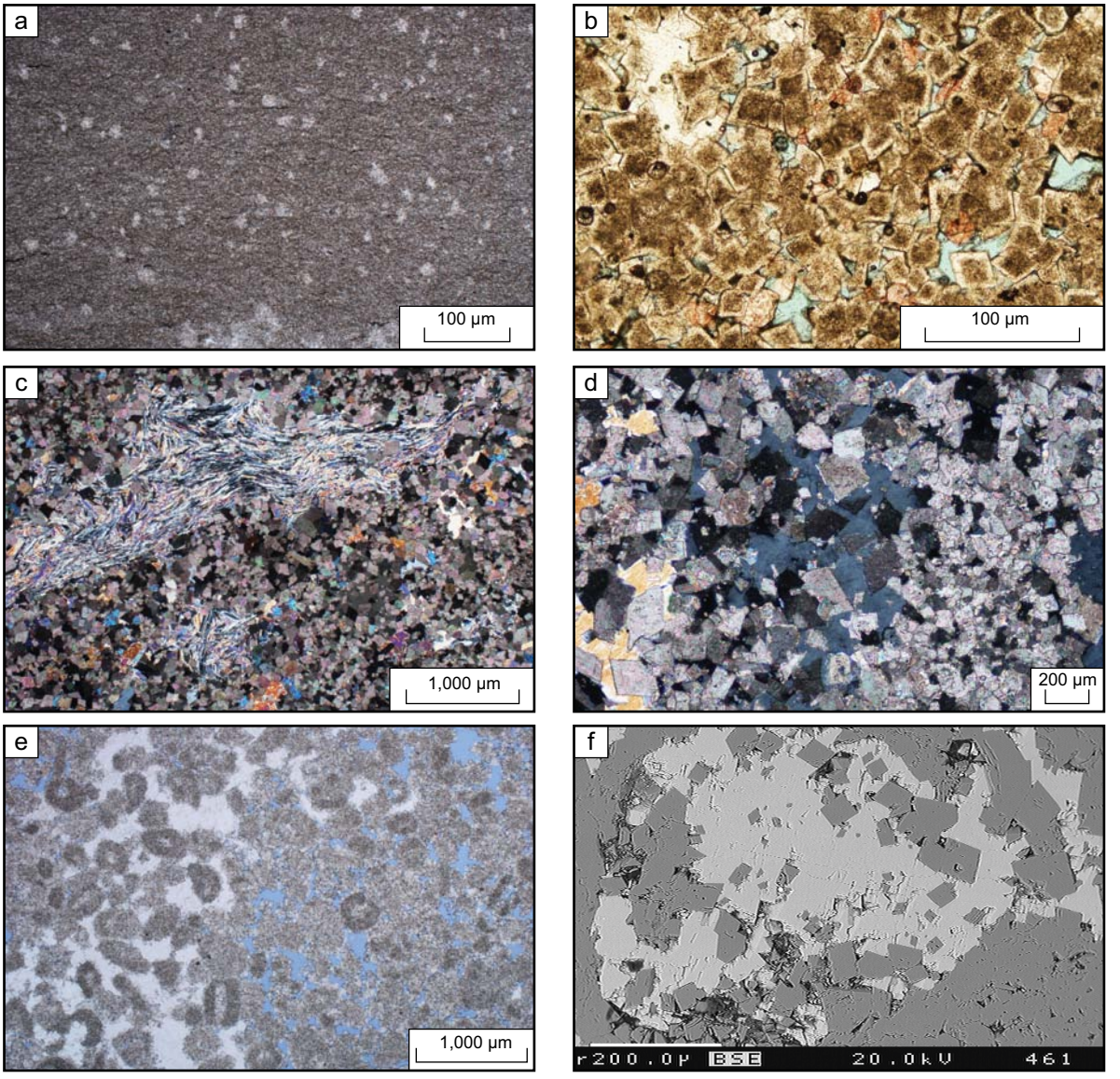

Figure 8: Optical photomicrographs and SEM images of dolostones: (a) Fine-crystalline dolostones with algal lamination. (b) Undifferentiated dolostone composed of inclusion-rich rhombic dolomite with limpid dolomite overgrowths. (c) Fine-crystalline peritidal dolomudstones with large patches of anhydrite cement (fibrous and felted crystals). Blocky anhydrite fills intercrystalline pore in adjacent dolostone. (d) Intercrystalline anhydrite and gypsum cements in undifferentiated dolostone (presumably dolomitized shoal grainstone); note that most of the dolomite rhombs are replaced by anhydrite and gypsum. (e) Intergranular anhydrite cement (light), which occurs in a dolograinstones formed by fairly fabric-preserving dolomitization. The presence of cemented and non-cemented patches in the dolostone is either due to partial dissolution or to incomplete cementation by anhydrite. (f) Backscattered electron image showing a moldic pore outlined by a layer of dolomite cement and filled by dolomite (grey) and anhydrite (light).

of inclusion-free quartz. The quartz cement contains rounded pores (ca. 50 µm across), which may indicate that silica has precipitated initially as opal. Silica cement is most common in HST of the Arab D3 and, to a lesser extent, in the HST of the Arab D4 and Arab D5.

Poikilotopic fluorite and celestine are rare cements, which fill intercrystalline and, less commonly, moldic pores. These cements are closely associated with anhydrite, which is engulfed and replaced by, and hence pre-dates, celestine. Fluorite engulfs, and hence post-dates these sulfate cements. Pyrite occurs in trace amounts as: (1) large euhedral crystals (up to 500 µm across), which engulf

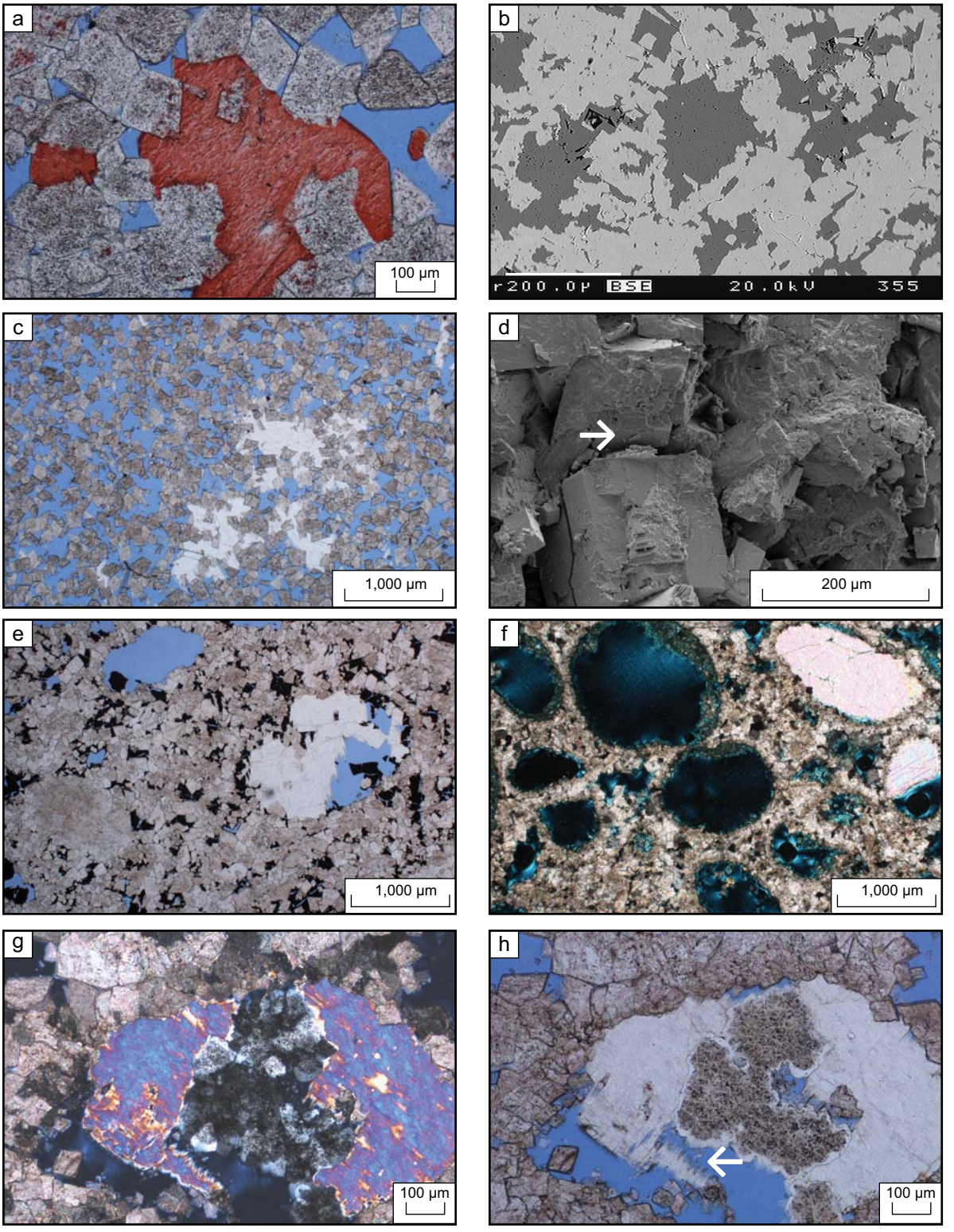

Figure 9: Optical photomicrographs and backscattered electron images of calcite cement and porosity in dolsotones, showing: (a) Coarse-crystalline calcite which fills intercrystalline pore between and replaces dolomite. (b) Severely calcitized (light) dolostone (grey). (c) Dolostone in which extensive sulfate cement (light) was dissolved leaving only scattered patches with etched boundaries. (d) Remnants of etched anhydrite cement (arrow). (e) and (f) Dolostones with scattered moldic pores in which the moldic pores contain partly dissolved anhydrite cement. (g) and (h) Companion images of a moldic pore filled by anhydrite, quartz and dolomite; anhydrite engulfs, and thus post-dates quartz and dolomite. Note that the anhydrite has been subjected to dissolution (arrow). The moldic pore is surrounded but not significantly filled by dolomite cement, suggesting that grain dissolution post-dates dolomite cementation. Some of the inclusions in the quartz are black, and are thus probably oil.

and pervasively replace dolomite crystals in the dolostones; and (2) framboids, which occur in the limestones and dolostones as individual crystals of ≤ 1 µm in size. Diagenetic K-feldspar occurs as extremely rare, tiny (≤ 10 µm in size) rhombohedral crystals in intercrystalline pores of the dolostones. Kaolin occurs as dickite polymorph as vermicular stacked pseudo-hexagonal crystals in LSW (unit D4M0) of one well, which is located along the present-day oil-water contact. Mg-rich smectite occurs as small, thin, curled flakes, which are engulfed by rhombic dolomite.

Stylolites occur in the anhydrite cemented dolostones and cut across the anhydrite crystals, which have replaced dolomite. Thus, stylolitization has occurred subsequent to formation of coarse-crystalline dolomite and anhydrite cement (Figure 10a). The presence of stylolites in dolostones with abundant intercrystalline porosity, which has resulted from the dissolution of intercrystalline anhydrite/gypsum cements, suggests that dissolution occurred subsequent to stylolitization. Bitumen and late calcite cement are encountered along the stylolites (Figure 10b).

All types of dolomite in the Arab Formation are non luminescent. Attempts to enhance the luminescence showed that in few cases the dolomite rhombs are dull to slightly dark red luminescent with thin non-luminescent rim. The dull luminescence is attributed to the nearly pure end member composition of the dolomite with nil Mn contents as revealed by EMP analyses.

ELECTRON MICROPROBE ANALYSES

EMP revealed that the various types of calcite cement have nearly pure end-member composition, with small amounts of Mg (nil to about 2 mole%) and commonly non-detectable amounts of Mn and Fe. The dolomite crystals, irrespective of texture, occurrence habits, and whether in limestones or dolostones, are Ca-rich ($CaCO_3$ = 52.2 and 58.8 mole%). Fe (bdl-30 ppm), Mn (bdl-30 ppm), and Sr occur in trace amounts or below the detection limits. The low concentrations of Fe and Mn suggest that the calcites have been formed under oxic to weakly reducing conditions (Froelich et al., 1979; Morad, 1998), assuming that oxides and oxyhydroxides of these metals occurred in the sediments. No systematic variations in the chemistry of diagenetic dolomite or calcite were detected related to occurrence habits across the field. (Major, minor and trace element data for the Arab carbonates are available from the authors upon request.)

STABLE CARBON, OXYGEN, AND STRONTIUM ISOTOPIC COMPOSITION

The isotope analyses (Figures 11a and 11b; carbon, oxygen and strontium isotopic data for the Arab carbonates are available from the authors upon request) have provided clues to the conditions encountered during dolomitization and calcite cementation. The $\delta^{18}O_{VPDB}$ values of fine-crystalline

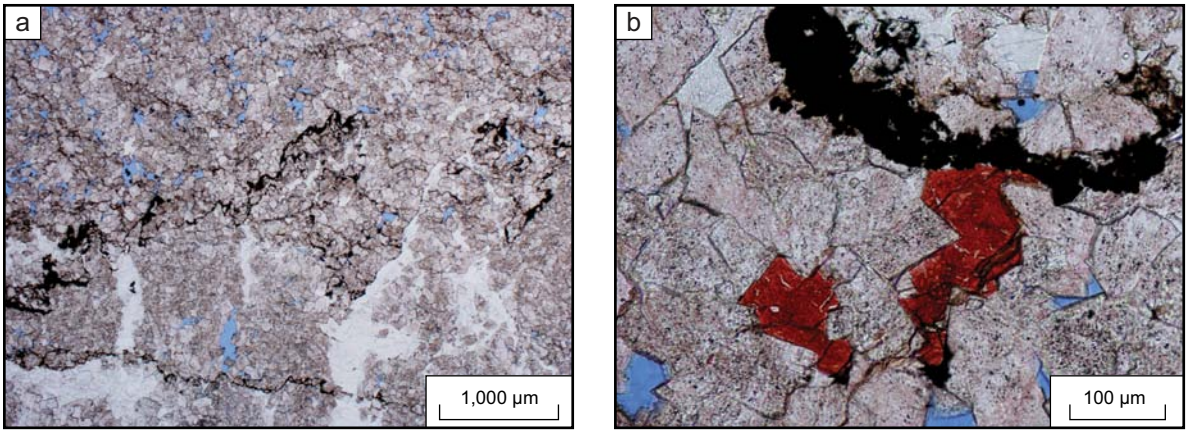

Figure 10: Photomicrograph (in PPL) showing (a) Bifurcating stylolites in dolostone cemented by anhydrite (light areas). Bitumen occurs along the stylolites which cut across the anhydrite cement. (b) Late intercrystalline calcite formed close to a stylolite with bitumen (black).

dolomite in sabkha-like carbonates vary between -2.9 and -0.1‰ and the $\delta^{13}C_{VPDB}$ values between +1.5‰ to +3.5‰ (Figure 11a). Medium-crystalline dolomite in dolostones has $\delta^{18}O_{VPDB}$ values between -5.8‰ to -0.7‰ and $\delta^{13}C_{VPDB}$ values from about +2.1‰ to +3.7‰ (Figure 11a). Coarse-crystalline dolomite has $\delta^{18}O_{VPDB}$ values from -6.7‰ to -4.1‰ and $\delta^{13}C_{VPDB}$ values from +1.0‰ to +3.7‰ (Figure 11a).

The isotopic signatures in calcitic components can be divided into three main groups (Figure 11b), including: (1) syntaxial rim calcite cement ($\delta^{18}O_{VPDB}$ from -5.4‰ to -3.5‰; $\delta^{13}C_{VPDB}$ = +2.0 to +3.1‰); (2) recrystallized peloids and matrix ($\delta^{18}O_{VPDB}$ from -6.2‰ to -3.4‰; and $\delta^{13}C_{VPDB}$ = +1.2 to +2.8‰); and (3) blocky/equant calcite ($\delta^{18}O_{VPDB}$ from -6.0‰ to -3.4‰, $\delta^{13}C_{VPDB}$ from +1.7‰ to 3.6‰). The three groups of calcite cements, despite their different formation timing within the diagenetic history of the basin, show overlapping O and C isotopic ratios; the carbon isotopic values are largely similar to those of Jurassic seawater. There is no systematic relationship between oxygen and carbon isotopes values and the systems tracts.

Syntaxial rim calcite cement reveals $^{87}Sr/^{86}Sr$ ratio varying between 0.70705 and 0.70752. The recrystallized peloids and matrix show $^{87}Sr/^{86}Sr$ ratios within the range of Jurassic carbonates and seawater values (Figure 12a). The $^{87}Sr/^{86}Sr$ ratios of blocky/equant calcite, which formed at a later diagenetic timing, are 0.70704-0.70743. The $^{87}Sr/^{86}Sr$ ratio of the fine-crystalline dolomite in sabkha-like carbonates (i.e. associated with patches and /or nodules of anhydrite/gypsum) ranges from 0.70701 to 0.70729 (Figure 12b). The $^{87}Sr/^{86}Sr$ ratio of medium-crystalline dolomite in dolostones ranges from 0.70709 to 0.7073 (Figure 12b). The $^{87}Sr/^{86}Sr$ ratio of coarse-crystalline dolomite, ranges from 0.707055 to 0.7077 (Figure 12b).

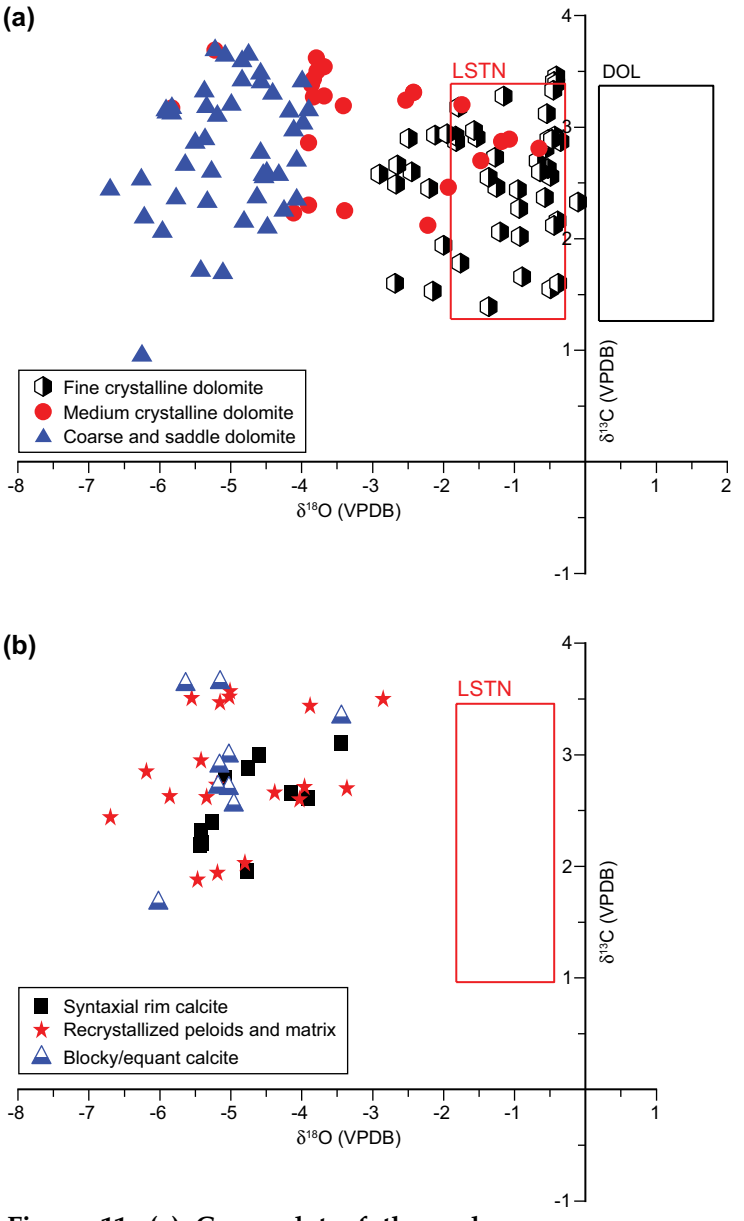

Figure 11: (a) Cross plot of the carbon *versus* oxygen isotopic signatures in various generations of dolomite of the Arab Formation showing their clear separation in oxygen isotopic signatures with progressive diagenetic alteration/formation. The rectangles DOL and LSTN represent the field of dolomite and calcite precipitated from Jurassic seawater (cf. Veizer et al., 1999). (b) Cross plot of the carbon *versus* oxygen isotopic signatures in the calcitic components. The rectangle LSTN represents the field of calcite precipitated from Jurassic seawater.

FLUID INCLUSION ANALYSES

Fluid inclusion analyses were performed on calcite, dolomite, and anhydrite, which attain various occurrence habits and paragenetic relationships. The analyzed calcite occurs as isopachous rim calcite cements (C1), syntaxial calcite overgrowths (C2) and equant calcite in intergranular and moldic

pores (C3), and coarse-crystalline calcite filling intercrystalline pores and replacing rhombic dolomite in dolostones (C4). The dolomite occurs as coarse-crystalline, inclusion-rich dolomite (DC2) and limpid dolomite cement rim or discrete crystals (DC3). The anhydrite analyzed occurs as nodules in dolomudstones (AN1), blocky intercrystalline and moldic pore-filling cement in dolograinstones (AN2), and blocky fracture-filling cement in dolostones and limestones (AN3).

Results of fluid inclusion petrographic and compositional analyses in calcite, dolomite, and anhydrite can be overall summarized as follows: (1) in most of the selected fluid inclusion assemblages (FIA), primary aqueous one-phase (all-liquid) and two-phase (liquid+vapour) fluid inclusions are present in a workable size for microthermometric analyses (average size 5 to 10 microns); (2) in the majority of the identified FIA, aqueous all-liquid and two-phase (liquid+vapour) fluid inclusions coexist; (3) the liquid to vapor ratio (L/V) in the two-phase inclusions appears moderately consistent within each FIA, with the area of the inclusion occupied by the vapour phase averaging 20–25% of the total volume.

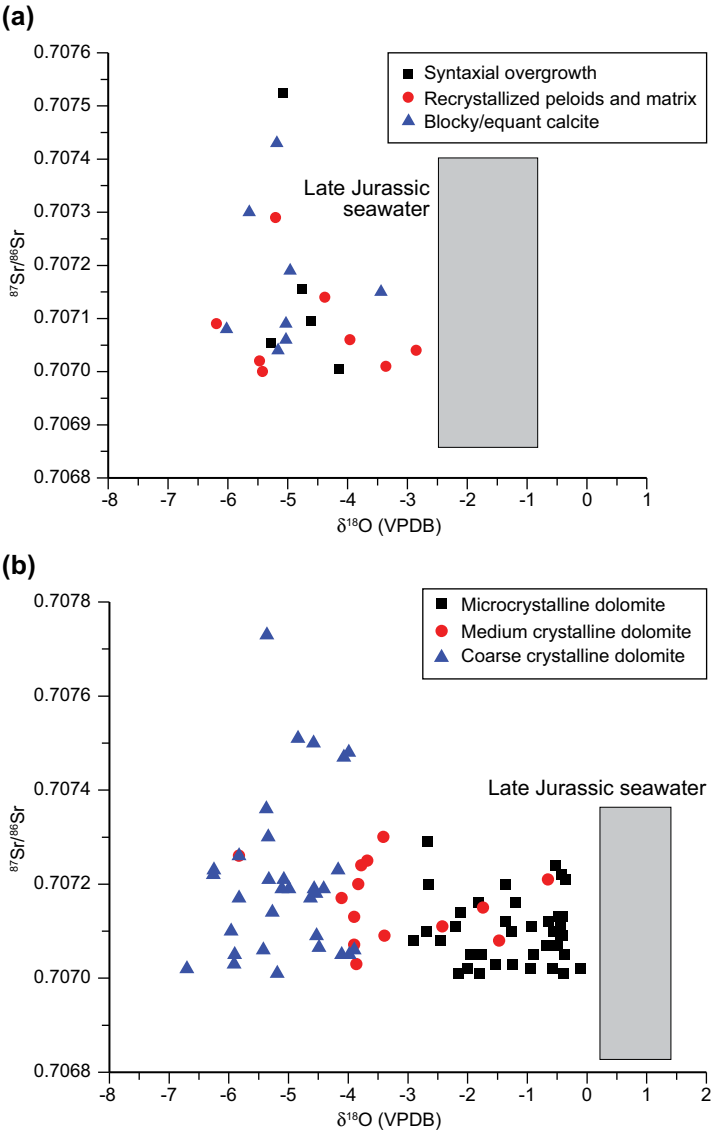

Figure 12: (a) Cross plot of $^{87}Sr/^{86}Sr$ ratios *versus* oxygen isotopes in calcite cements of the Arab Formation showing the similarity to Jurassic seawater values in $^{87}Sr/^{86}Sr$ ratios but comparable oxygen isotopic values. The rectangle represents the field of calcite precipitated from Jurassic seawater. (b) Cross plot of $^{87}Sr/^{86}Sr$ ratios *versus* oxygen isotopes in the dolostones of the Arab Formation showing the overlapping akin to Jurassic seawater values in $^{87}Sr/^{86}Sr$ ratios but different oxygen isotopic values. The rectangle represents the field of dolomite precipitated from Jurassic seawater.

Primary and secondary petroleum fluid inclusions were found in dolomite (DC2) and late anhydrite cements (AN2 and AN3). DC2 dolomite cores contain tiny, yellow to green fluorescent oil inclusions, whereas the rims (DC3) are inclusion free or inclusion poor (Figures 13a and 13b). The presence of oil inclusions in the dolomite core is interpreted to indicate that this dolomite (DC2; Figures 13c and 13d), which is paragenetically earlier than the limpid dolomite (DC3), has been formed during an early phase of oil migration, whereas the limpid, non-fluorescent rim has precipitated during a pause in oil migration. In addition to fluorescence caused by the presence of oil inclusions, the fluorescence of dolomite core (DC2) suggests precipitation from formation waters rich in dissolved organic acids (Neuweiler et al., 2003). The nodular sulfate (AN1) is characterized by aqueous, all liquid inclusions, but in rare cases liquid and vapor phases are encountered. The blocky, intercrystalline (AN2) contains rare oil inclusions whereas fracture-filling anhydrite/gypsum cements (AN3) often contain large oil inclusions (Figures 13e–f) displaying yellowish green and whitish blue fluorescent color under UV-light observations.

Results of compositional analyses have revealed three types of oil inclusions, which display a yellowish, greenish, and bluish fluorescence colors, suggesting that oil migration into the reservoir occurred during stages of progressive increase in organic matter maturation in the source rocks. The yellowish and greenish colored inclusions are indicative of a medium- to heavy oil (API 20–40°), being restricted

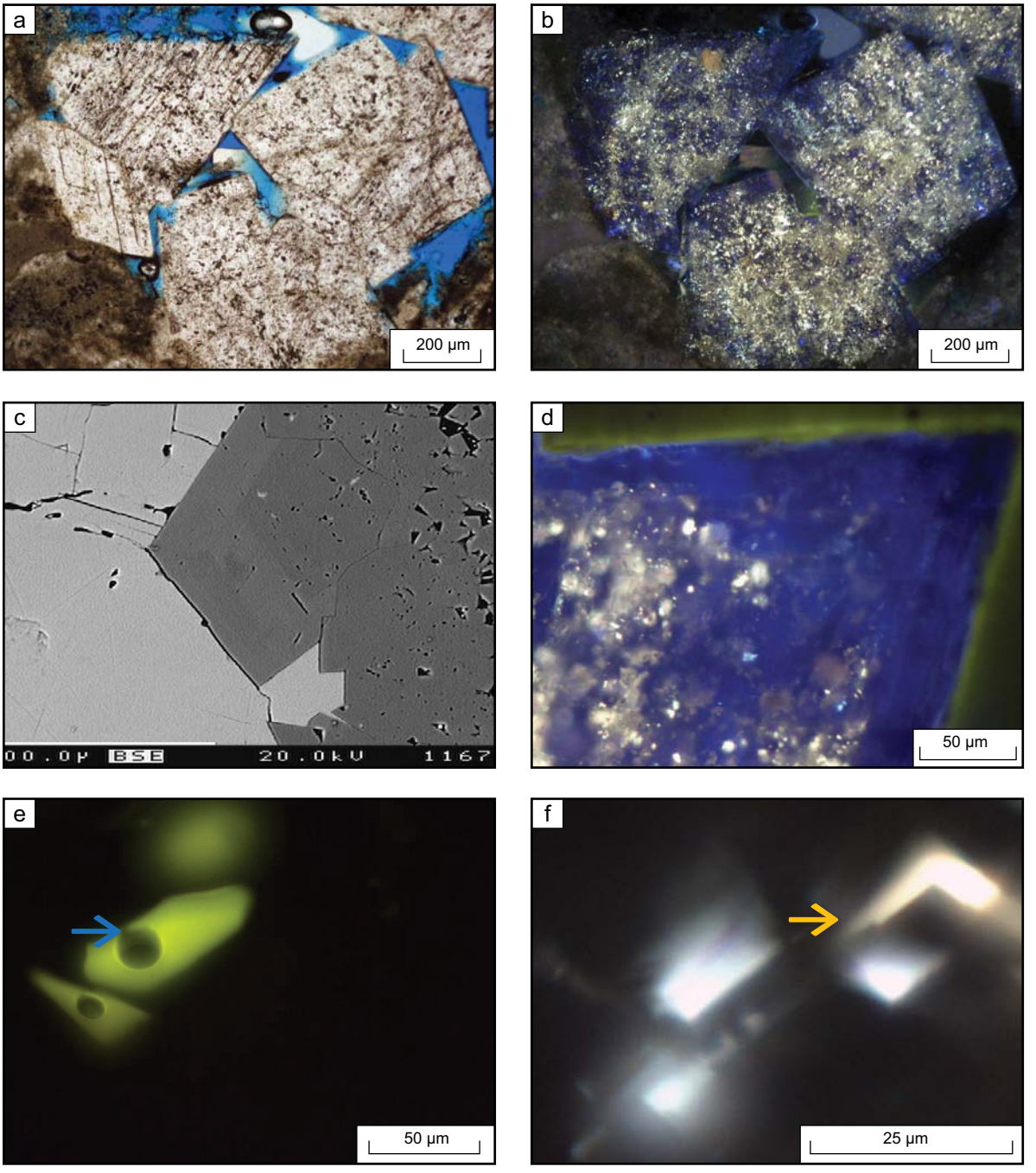

Figure 13: (a) Photomicrograph (PPL) showing inclusion-rich dolomite (DC2) with inclusion-poor rim (DC3) and (b) The same view (UV light) showing that the core and contains yellow fluorescent oil inclusions. (c) Backscattered electron image (BSE) showing the limpid dolomite rim is brighter grey due to slightly higher Sr content than the dolomite core. (d) Fluorescence image showing inclusion-free DC3 rim. Note yellow fluorescent oil inclusions present in the inclusion-rich dolomite core. (e) Large inclusion filled with yellowish-green fluorescing oil inclusion with gas bubble (arrow) in the late fracture-filling anhydrite. (f) Whitish blue color fluorescing oil inclusion (arrow) in fracture-filling anhydrite.

to the inclusion-rich dolomite cores (DC2.) The greenish and bluish colored inclusions occur in the late-diagenetic, fracture-filling anhydrite/gypsum (AN3), which are indicative of medium-light oils (API 30–50°; McLimans, 1987).

Microthermometry

The homogenization temperatures (T_h) and salinities measured in the fluid inclusions for the various diagenetic phases (Figure 14) showed high T_h and highly saline fluids in calcite cements in the limestones (C1, C2 and C3). The T_h values range from 74.4° to 111.6°C (average 84.1°C) for C1 and C2 cements and from 80.9° to 108.5°C (average 94.5°C) for C3 cement. Fluid salinity ranges between 11.6 and 16.8 (average 13.6) wt% NaCl equivalent for C1 and C2 cements and 9.1 to 16.9 (average 13.3) wt% NaCl equivalent for C3 cement. Primary, all-liquid fluid inclusions, which mostly occur in early-diagenetic syntaxial calcite overgrowths (C2) and equant bladed calcite (C3), may record low temperatures of precipitation (below about 50°C; Goldstein, 2001). Conversely, the presence of two-phase inclusions in the same FIA could indicate that some of the fluid inclusions in this texturally early-diagenetic calcite were thermally re-equilibrated and leaked and re-filled during burial diagenesis. This interpretation is supported by the wide distribution of the microthermometric data (Figure 14). Therefore, the temperatures measured for C1, C2 and C3 are not reliable. Precipitation of the blocky C4 calcite cement and concomitant re-equilibration of fluid inclusions in calcites C1, C2 and C3 have presumably occurred during burial diagenesis.

The T_h in inclusion-rich dolomite (DC2) range from 61.8° to 98.2°C (average 83.1°C) and salinity ranges from 9.9 to 15.5 wt% NaCl eq. (average 13.3 wt%). Fluid inclusions in dolomite cements (DC3) reveal a narrow range of T_h (93.8° to 104.0°C; average 100.5°C); salinity values vary from 16.3 to 19.0 wt% NaCl equivalent (average 17.6 wt%). The blocky calcite cement (C4), which fills intercrystalline and vug pores in the dolostones, display a wide range of T_h (54.0° to 133.5°C; average 87.2°C) and salinities (12.3 to 21.3 wt% NaCl eq.; average 16.2 wt%). The wide range of T_h and salinities suggest the impact of thermal re-equilibration owing to leakage and refilling of the inclusions in this cement phase.

Fluid inclusion temperature and salinity data (T_h = 90.4° to 122.4°C; average 105.9°C and salinity = 16.3 to 23.0 wt% NaCl eq.; average 19.9 wt%) from blocky intercrystalline and moldic pore-filling anhydrite cement in the dolograinstones, and blocky fracture-filling anhydrite in dolostones and limestones (Figure 14) are similar to those in brines presently occurring in the reservoir (T_h = 110.0°C and formation waters salinity of 20.3 wt% NaCl). Finally, it has been noted that there is a general increase in homogenization temperatures and salinities in cements of the dolostones according to the paragenetic order of precipitation.

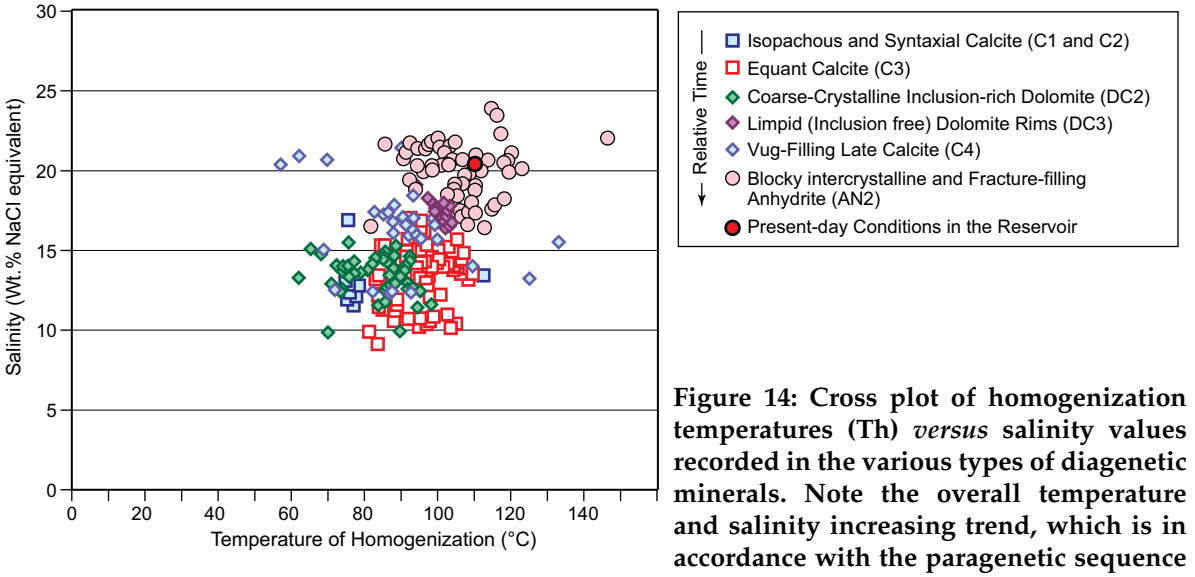

Figure 14: Cross plot of homogenization temperatures (Th) *versus* salinity values recorded in the various types of diagenetic minerals. Note the overall temperature and salinity increasing trend, which is in accordance with the paragenetic sequence of diagenetic events. The distribution in calcite (C4) deviates from the trend, probably due to re-filling of the fluid inclusions with waters of different salinities during burial diagenesis.

FORMATION WATER CHEMISTRY

The present-day formation waters (Elhami, personal communication, 2010) are extemely saline (TDS = 203,550 mg/L) and dominated by Na (78,400 mg/L) and Cl (118,480 mg/L). Other cations include K (555 mg/L), Ca (270 mg/L), Mg (215 mg/L), and trace amounts of Sr (11 mg/L). Dissolved barium and iron occurs in concentration < 1 mg/L. Other anions include sulfate (4,860 mg/L), bicarbonate (760 mg/L) and trace amounts of boron (2.5 ppm). No aluminum, silicon, phosphate or lithium was detected. The gases analyzed include mostly methane with smaller amounts of propane, whereas H_2S, CO_2 and other gases occur in trace amounts.

DISCUSSION

The petrographic observations complemented by geochemical analyses and fluid-inclusion microthermometry have allowed us to: (1) construct a paragenesis and establish the formation conditions of the main diagenetic events in the limestones as well as in the dolostones (Figure 15); the diagenetic regimes are used after Choquette and Pray (1970); (2) unravel the impact of the main diagenetic alterations on reservoir porosity and permeability; and (3) develop a conceptual model linking the distribution of diagenetic alterations and of their impact on reservoir quality to the sequence-stratigraphic framework.

Paragenetic Sequence

The sequence of diagenetic processes in the limestones includes:

(1) syn-depositional to eogenetic micritization of the allochems and development of thin micrite envelopes around the grains.

(2) Eogenetic precipitation of isopachous calcite rim around the allochems and of syntaxial calcite overgrowths around echinoids grains in the grainstones. Spalling of the isopachous grain rims is presumably caused by mechanical compaction.

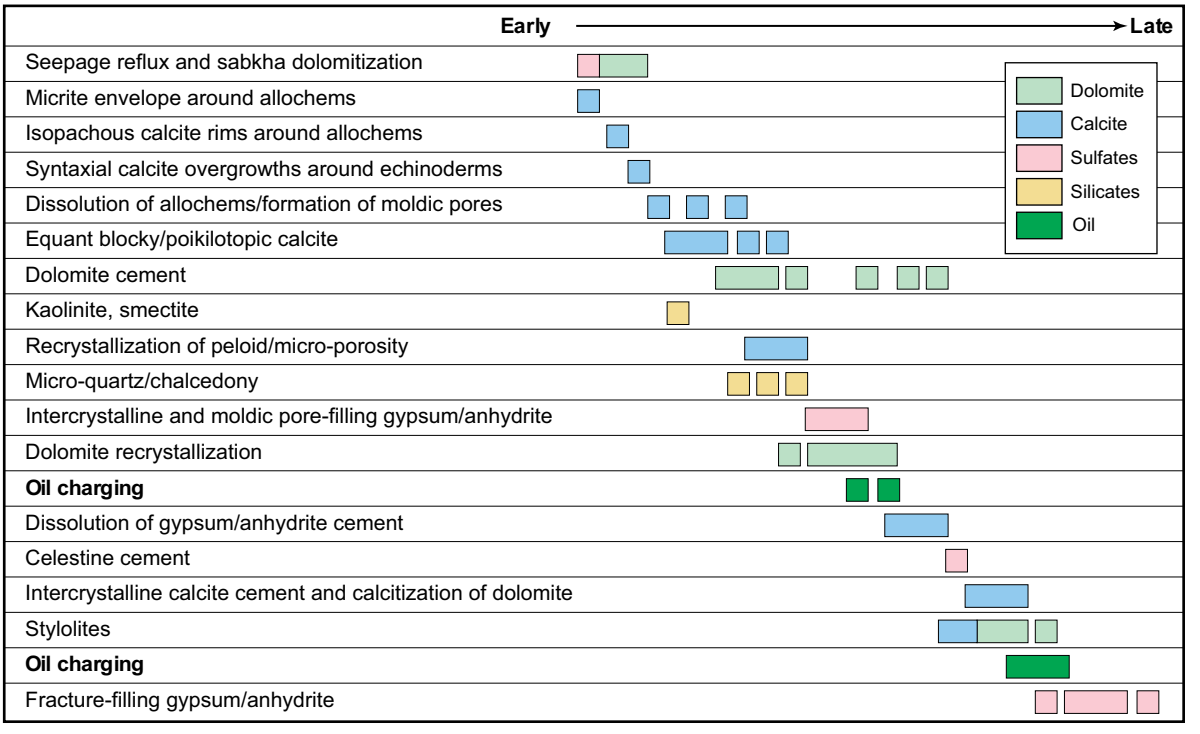

Figure 15: General paragenetic sequence reconstructed for the Arab Formation. Two main episodes of oil charging into the reservoir have been inferred.

(3) Eogenetic partial to pervasive dolomitization of bioturbated lime mudstones and lime wackestones below surfaces of marine transgression (e.g. MFS). The formation of small amounts of scattered framboidal pyrite is suggested to be formed by bacterial sulfate reduction.
(4) Eogenetic silicification (replacement by micro-crystalline quartz/chalcedony), which resulted in the formation of silica nodules primarily in limestones deposited in the outer ramp. The required silica was presumably derived from the dissolution of sponge spicules, which are most common in the outer ramp sediments.
(5) Eogenetic dissolution of framework grains and formation of intragranular/moldic pores in the packstones and grainstones, and cementation by equant calcite in the intergranular and intragranular/moldic pores in the grainstones and rudstones presumably owing to meteoric flux below sequence boundary. The formation of equant calcite cement may have continued during burial diagenesis and was accompanied by partial dissolution and recrystallization of mud matrix and peloids resulting in the formation of micro-porosity.
(6) Mesogenetic formation of scattered rhombic crystals by replacement of peloids and filling of adjacent intergranular pore space as well as by selective replacement of syntaxial calcite overgrowths, which were developed around the echinoids grains.
(7) Mesogenetic cementation by grain- and cement-replacive gypsum and anhydrite, which were mobilized along fractures associated with faults. The timing of stylolites development is uncertain, but may have been initiated at relatively shallow depths (few hundreds of meters to ca. 1 km).

Paragenetic sequence of diagenetic processes in the dolostones includes:
(1) eogenetic (near-surface to very shallow burial) dolomitization of the supratidal, lagoonal and shoal coarse-grained carbonate sediments. Dolomitization of the peritidal sediments was closely associated with the formation of anhydrite/gypsum nodules. Dolomitization was mostly fabric destructive, with fine- to coarse-crystalline texture in the grainstones of the shoal and microcrystalline in the peritidal mudstones to wackestones. The formation of trace amounts of kaolinite and smectite, which pre-dates rhombic dolomite, occurred locally. Smectite forms under arid climatic conditions, whereas kaolinite forms in wet climatic conditions (Morad et al., 2000). Hence, there may have been shifts in the climatic conditions during deposition of the Arab Formation. Diagenetic clay minerals in carbonate successions commonly form by meteoric-water diagenesis at and below surfaces of subaerial exposure.
(2) Eogenetic formation of moldic pores has probably occurred by dissolution of aragonite allochems. Grain dissolution was also accompanied or followed by dolomitization of the Arab Limestones.
(3) Eogenetic to mesogenetic precipitation of discrete, rhombic micro-crystalline dolomite in moldic pores in the wackestones and of coarser crystalline, discrete or drusy dolomite in the grainstones. The latter dolomite has also precipitated as limpid overgrowths around the inclusion-rich dolomite (cf. Machel, 2004). The limpid rims may represent syntaxial overgrowths (Choquette and Hiatt, 2008) resulting from over-dolomitization (Jones and Xiao, 2005). Similar late diagenetic dolomite types in carbonate successions have been reported in other carbonate successions (Kupecz and Land, 1991; Varol and Magaritz, 1992).
(4) Precipitation of quartz, which engulfs and replaces the rhombic, moldic pore-filling dolomite; the required silica was probably derived intraformationally from the dissolution of sponge spicules or from extra-formational basinal brines. The formation of rare small crystals of K-feldspar was probably aided by the evaporative, K-rich, marine brines.
(5) Precipitation of coarse-crystalline anhydrite and gypsum in the intercrystalline and moldic pores of the dolostones; these sulfate minerals replace the rhombic dolomite partly to extensively. Cementation by minor celestine was probably a consequence of the conversion of gypsum into anhydrite (Tucker and Wright, 1990) and contemporaneous partial dissolution of anhydrite and gypsum, which contain up to 10,000 ppm Sr. It has been argued that celestine and anhydrite are common diagenetic minerals, which are formed during dolomitization by evaporative brines (Bush, 1973).
(6) Stylolite development, which affected the dolomite cement types and coarse blocky anhydrite. Stylolites in dolostones develop at greater depths than in limestones.
(7) Dissolution of intercrystalline and moldic pore-filling anhydrite, primarily in the dolograinstones and concomitant precipitation of small amounts of celestine in the intercrystalline pores between dolomite crystals.
(8) Cementation by coarse-crystalline, blocky calcite in the moldic pores, which has replaced the dolomite crystals to variable extents.

(9) Precipitation of minor amounts of fluorite and coarse-crystalline, grain and cement replacing pyrite.
(10) Major phase of oil emplacement, which virtually completely inhibited further diagenetic process except for late anhydrite and gypsum cementation along fractures associated with faults, which occurred at near present-day bottom-hole temperatures (BHT) and salinity of formation waters. Carbonate reservoirs are overall oil wet in fully oil-charged reservoirs (Barclay and Worden, 2000).

The high homogenization temperatures obtained for all diagenetic minerals even for the texturally early diagenetic syntaxial calcite overgrowths, isopachous calcite rim, and equant calcite suggest that these calcite phases as well as the various types of dolomite have suffered from recrystallization and concomitant isotopic and fluid inclusion resetting. Recrystallization of calcite and dolomite during burial diagenesis is a widely recognized phenomenon in carbonate successions (Choquette and James, 1987; Mazzullo, 1992; Malone et al., 1994; Machel et al., 1996).

The presence of very small amounts of coarse-crystalline, late pyrite can be attributed to the iron-poor composition of the Arab Formation sediments. Such pyrite is commonly suggested to be formed during mesodiagenesis where the sulfide ions are derived from thermal sulfate reduction (TSR; Worden et al., 1996). The framboidal pyrite, which is encountered mainly in the limestones, is suggested to be formal by bacterial sulfate reduction during near-surface eodiagenesis (Morad, 1998).

The diagenetic processes in the sulfate nodules and beds are simpler than those in the limestones and dolostones, and include conversion of gypsum into anhydrite and development of stylolitic surfaces; both of these processes are promoted by increase in temperature.

Dolomitization Models in the Arab Formation

Dolomitization, in general, is still a topic of considerable controversy and debate (Warren, 2000; Machel, 2004). The close association of anhydrite/gypsum beds, nodules, and cements with dolostones of the Arab Formation suggests that dolomitization occurred by evaporative increase in salinity and density of seawater, which was promoted by arid climatic conditions (Adams and Rhodes 1960; Machel, 1986; Kaufman, 1994; Gill et al., 1995; Meyers et al., 1997; Jones and Xiao, 2005; Swart et al., 2005).

Dolomitization of the peritidal sediments of the Arab Formation is suggested to occur according to the sabkha model. Seepage reflux dolomitization is inferred for dolomitization of sediments in the subtidal, shoal, and lowstand wedge. Dolomitization may have occurred by means of brines

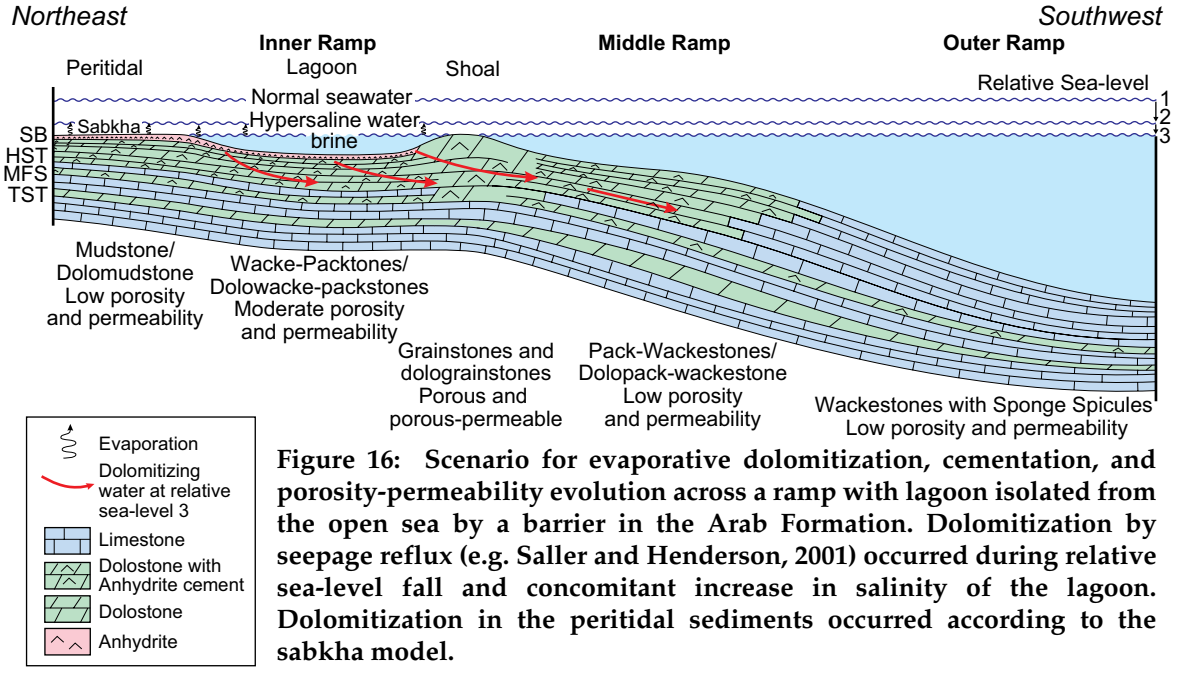

Figure 16: Scenario for evaporative dolomitization, cementation, and porosity-permeability evolution across a ramp with lagoon isolated from the open sea by a barrier in the Arab Formation. Dolomitization by seepage reflux (e.g. Saller and Henderson, 2001) occurred during relative sea-level fall and concomitant increase in salinity of the lagoon. Dolomitization in the peritidal sediments occurred according to the sabkha model.

derived from evaporation of seawater in a lagoon, which was semi-isolated from the open sea by a shoal barrier (Figure 16). The removal of Ca^{2+} from seawater through the precipitation of sulfate beds, nodules, and cements in the evaporative settings of the Arab Formation, which results in increase in the Mg^{2+}/Ca^{2+} in porewater and lagoon brines, may have promoted dolomitization (Tucker and Wright, 1990). Furthermore, it has been suggested that dolomite stabilization is accelerated by the removal of sulfate ions (through the precipitation of the above mentioned sulfates), which may have an inhibiting effect on dolomite formation (Baker and Kastner, 1981; Morrow and Ricketts, 1988; Slaughter and Hill, 1991; Mazzullo, 2000).

The development of such a dolomitization-prone depositional environmental setting is anticipated to have occurred during a major fall in the relative sea level, promoted by the arid climatic conditions. Dolomitization associated with reflux from superjacent peritidal sediments has been suggested to typically affect only the upper 0.3–3 ft of strata (Machel, 1986), whereas geochemical modeling indicates that reflux dolomitization may extend to depths of ca. 3,300–6,600 ft (Jones et al., 2003).

The paragenetic sequence of diagenetic alterations by seepage reflux of brines in the Arab Formation includes (Machel, 1986; Morrow, 2001; Jones and Xiao, 2005): (1) dolomitization of allochems and matrix and concomitant creation of intercrystalline and moldic/intragranular porosity in the subtidal, shoal and slope sediments; (2) cementation of the moldic pores by discrete dolomite crystals; and (3) cementation of intercrystalline pores in the dolostones by anhydrite and gypsum, which is promoted by the previous dolomitization events resulting in Ca^{2+}/Mg^{2+} increase in the pore water.

The isotopic signatures of dolomite suggest that dolomitization occurred from slightly modified marine pore waters and/or at slightly elevated temperatures than that of ambient seawater. The carbon isotopic signatures are similar to those inferred for Jurassic seawater (+1‰ to +3‰; e.g. Veizer et al., 1999). The relatively wide range and lower $\delta^{18}O_{VPDB}$ values than those anticipated for dolomite formed from Jurassic seawater are attributed to the presence of variable amounts of later diagenetic dolomite, partial recrystallization, and the presence of thin dolomite overgrowths (cf. Al-Aasm, 2000). The carbon isotopic signatures for medium- and coarse-crystalline dolomite indicate that dissolved carbon was derived to a large extent from the host carbonate deposits. The $^{87}Sr/^{86}Sr$ ratio of the fine-crystalline dolomite in sabkha-like carbonates (i.e. associated with patches and/or nodules of anhydrite/gypsum) ranges from 0.70701 to 0.70729 (Figure 12a). These values are similar to those of Jurassic seawater indicating that precipitation occurred from marine pore waters with no evidence of involvement of meteoric fluids.

Using the fluid inclusion T_h in conjunction with the range of $\delta^{18}O$ composition for various generations of dolomite and the dolomite-water fractionation equation (Land, 1983), the $\delta^{18}O_{V\text{-}SMOW}$ composition of the precipitating fluid for coarse-crystalline limpid dolomite would have varied between +3.5‰ and +6.5‰; while the $\delta^{18}O_{V\text{-}SMOW}$ composition of the precipitating fluid for medium-crystalline dolomite ranges from +2.5‰ and +5.5‰ (Figure 17a). In contrast, the earliest type of dolomite shows lower T_h and drastically different salinities. The presence of mostly or only liquid-filled inclusions in the fine-crystalline dolomite and its association with sabkha facies suggest formation during early diagenesis at near-surface temperatures. However, this dolomite has been recrystallized to various extents as evidenced from petrographic observations and slightly depleted $\delta^{8}O_{VPDB}$ values compared to the postulated composition for dolomite formed from Jurassic seawater.

Origin of Burial Dolomite, Quartz, and Calcite Cements and Causes of Sulfate Dissolution

The limpid characteristics and elevated formation temperatures (T_h > 90ºC) of dolomite overgrowths and medium- to coarse-crystalline dolomite (DC3), which commonly occupy the central parts of moldic pores has presumably occurred during a pause in hydrocarbon migration (Mountjoy and Amthor, 1994; Al-Aasm, 2000; Machel and Hubscher, 2000). Conversely, the presence of abundant oil inclusions in the dolomite cores DC2 (T_h = 85–100°C) suggests formation during hydrocarbon migration, probably during the initial stages of emplacement of Oman ophiolites (Late Cretaceous) (Ali and Watts, 2009). However, organic geochemical analyses indicate that the peak oil generation

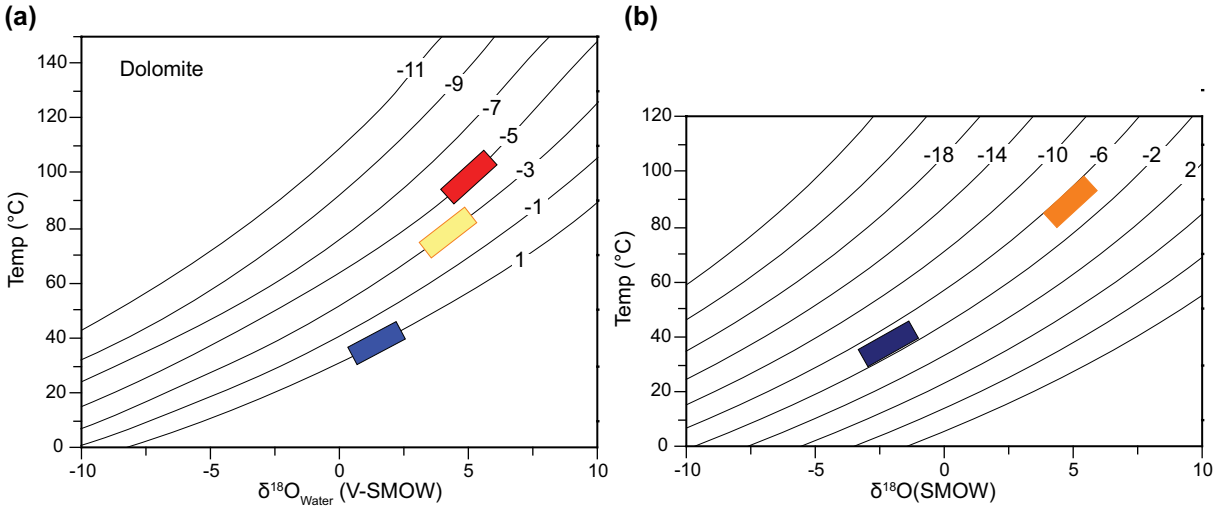

Figure 17: (a) Oxygen isotope values of various dolomite generations are plotted on the temperature dependent, dolomite-water oxygen fractionation curve. The formation temperatures of dolomite are based on fluid inclusion micro-thermometry. Temperature of precipitation of eogenetic dolomite (blue rectangle) is assumed to be those of near-surface conditions. The medium crystalline dolomite (yellow rectangle) and coarse crystalline dolomite (red rectangle) record higher temperature of formation and more enriched $\delta^{18}O_{SMOW}$ values. (b) Oxygen isotope values of various calcite generations are plotted on the temperature dependent, calcite-water oxygen fractionation curve. The formation temperatures of dolomite are based on fluid inclusion micro-thermometry. Using the range of homogenization temperatures of late diagenetic calcite (orange) indicate formation from evolved brines.

and charging of hydrocarbon occurred during the Eocene and that oil was sourced from the Jurassic source rock of Hanifa Formation. This possible multiple sources of oil may explain the two main types of oil entrapped in the fluid inclusions of dolomite and sulfate cement.

Fluid inclusions data (T_h = 90.4° to 122.4°C; average 105.9°C and salinity = 16.3 to 23.0 wt% NaCl eq.; average 19.9 wt%) from blocky intercrystalline and moldic pore-filling anhydrite cement in the dolograinstones, and blocky fracture-filling anhydrite in dolostones and limestones (AN2) suggest precipitation from hot brines, similar to those presently occurring in the reservoir (T_h = 110.0°C and formation waters salinity of 20.3 wt% NaCl).

There are two possible origins for the formation of calcite (C4) in the dolograinstones, calcitization of dolomite, and dissolution of anhydrite. These origins include: (1) incursion of undersaturated meteoric fluids into the sediments (Morad et al., 2000, 2011), and (2) thermal sulfate reduction (TSR). The high T_h and salinities of fluid inclusions in these calcites (T_h ca. 75–105°C; salinity ca. 14–18 wt% NaCl equivalent) suggests a mesogenetic origin (Figure 14). This would mean that meteoric water flux could have occurred during uplifting caused by the obduction of Oman ophiolites (Ali and Watts, 2009). However, maintainance of the undersaturation state of meteoric waters would be difficult to achieve taking into account the enormous buffering capacity of the thick carbonate successions. Using T_h and $\delta^{18}O_{VPDB}$ values of C4 calcite cement, and employing the calcite-water oxygen isotope fractionation equation (Freidman and O'Neil, 1977), it is inferred that cementation occurred from pore waters with $\delta^{18}O_{SMOW}$ values of +3.5 to +6.5‰, which are typical values for basinal brines in evaporative settings (Figure 17b) (Egeberg and Aagaard, 1989) and resembles those obtained for the dolomite cements. The textural mesogenetic origin of calcite suggests that TSR is a most likely explanation. TSR occurs indeed in the underlying Permian–Triassic Khuff Formation (Worden et al., 1996). TSR leads to decrease in the salinity of formation waters and calcite cementation (Worden et al., 1996). Thus, episodic flux of these formation waters along fractures associated with faults may have caused salinity perturbation in the Arab Formation. The partial to pervasive replacement of dolomite by this late blocky calcite supports the hypothesis of TSR (Cantrell et al., 2007; Nader et al., 2008).

Dolostones containing calcitized dolomite and late calcite cement do not occur in the close vicinity of sequence boundaries, which preclude the role of meteoric-water flux below subaerial exposure surfaces. Yet, several lines of evidence preclude the role of TSR in the dissolution of anhydrite and gypsum cements in the Arab Formation: (1) the lack of elemental sulfur, which is a by-product of TSR (Machel, 1987; Worden and Smalley, 1996; Worden et al., 1996; Machel and Buschkuehle, 2008); (2) the lack of calcitized sulfate cement; (3) the relatively low homogenization temperature (ca. 75ºC) of some intercrystalline calcite cement, which is closely associated with the dissolved sulfate cements; and (4) the lack of negative $\delta^{13}C$ values in the precipitated calcite cement (Machel and Buschkuehle, 2008).

Replacement of dolomite by intercrystalline anhydrite and gypsum was presumably promoted by elevated Ca^{2+}/Mg^{2+} activity ratio and SO_4^{2-} activity, which destabilizes dolomite (Baker and Kastner, 1981). The formation of celestine cement is attributed to the release of strontium from the dissolution of anhydrite and gypsum as well as from the dissolution and stabilization of aragonite to low-Mg calcite. The latest cement generation in the formation is fracture-filling anhydrite and gypsum (T_h mostly 105–120°C; salinity 16–22 wt% NaCl), which was formed during the second phase of oil migration as evidenced by the frequent presence of oil inclusions. The formation of this cement is most likely still ongoing, which is supported by similar salinities in the fracture-filling sulfates and present-day formation waters and T_h close to bottom-hole temperatures.

Impact of Diagenesis on Reservoir-Quality Evolution

Diagenetic alterations in the Arab Formation have overall accentuated the reservoir quality heterogeneity. Complete dolomitization in the supratidal mudstones has resulted in increase in porosity (up to 12%) but either no or minor improvement of permeability (up to 75 mD) compared to the precursor impermeable carbonate mud (cf. Smith et al., 2004). Dolostones with abundant poorly-connected moldic/intragranular porosity due to extensive cementation of the intergranular pores by dolomite have lower permeability (< 5 mD) than that of the original grainstone. Many of the dolostones with microcrystalline or medium-crystalline texture with tightly interlocked dolomite crystals of undifferentiated origin are characterized by low-porosity (< 5%) and low-permeability (< 10 mD). Conversely, coarse-crystalline undifferentiated dolostones or dolograinstones, which are characterized by well-connected intercrystalline and moldic porosity, have on average high porosity (ca. 20%) and high permeability (ca. 830 mD). Grainstones in which the grains are not dolomitized but intergranular pores are nearly completely occluded owing to compaction and cementation have nil porosity and permeability.

The presence of partly to pervasively dissolved dolomite crystals in the dolostones is interpreted to represent remnants of dolomite crystals, which were earlier replaced to various extents by intercrystalline anhydrite cement. The dissolved dolomite crystals were left behind subsequent to the dissolution of anhydrite cement. Evidence supporting this postulation includes the engulfment, but not the complete filling of pores after dissolved dolomite by anhydrite showing evidence of partial dissolution.

A cross plot of porosity *versus* permeability, with different groups based on various extents of dolomitization (replacive and cement types) in the Arab Formation carbonate rocks (Figure 18) shows that dolomitization has varied patterns of impact on reservoir quality resulting in wide ranges of porosity and permeability. The plot further reveals that there is a significant positive correlation between porosity and permeability for the whole data set. The wide range of permeability values for a certain porosity value and vice versa is attributed to the presence of variable amounts of micro-porosity and/or variable amounts of moldic and intragranular pores, which are poorly inter-connected with the overall pore system of the rock. The best reservoir rocks in the Arab Formation include: (1) Shoal grainstones, which contain substantial amounts of moldic and intragranular pores, and in which the depositional intergranular porosity was preserved owing to the presence of small amounts of scattered syntaxial calcite overgrowths, rhombic dolomite, and/or equant calcite. These cements have supported the grainstones framework and thus inhibited pervasive compaction of the abundant ductile peloids. (2) Medium- to coarse-crystalline shoal dolograinstones with abundant, well-connected intercrystalline porosity. In many cases, these dolostones have undergone improvement of reservoir quality by dissolution of intercrystalline gypsum and anhydrite cements.

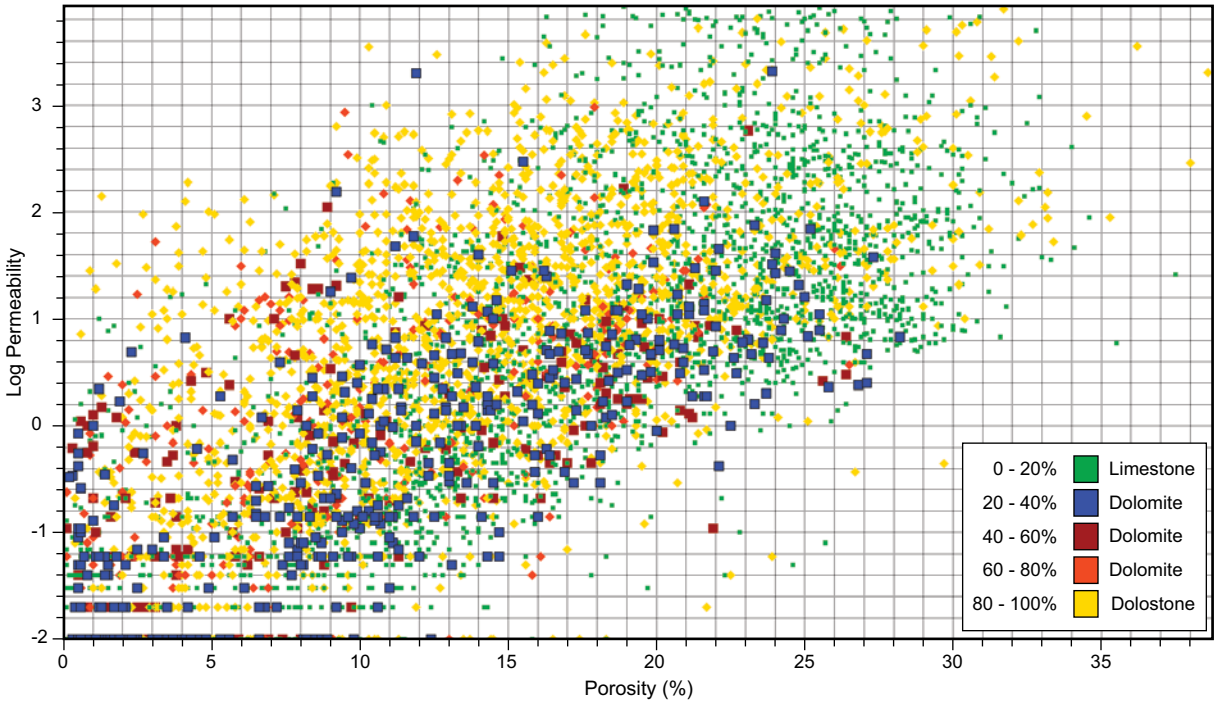

Figure 18: Cross plot of fluid porosity *versus* log permeability for carbonate rocks of the Arab Formation based on the percentages of dolomite. The plot shows a significant positive correlation between porosity and permeability for each category representing % of dolomitazation.

The reservoir quality evolution of the limestone has been affected by the following processes:

(1) reservoir-quality destruction by grain compaction (mechanical and chemical) and cementation of inter- and intragranular/moldic pores. Mechanical compaction of peloidal grainstones has resulted on average in porosity of ca. 12% and permeability < 3 mD. Pervasive cementation of grainstones and rudstones by equant calcite or, less commonly, dolomite resulted in moderate porosity (ca. 10–15%) and low permeability (< 5 mD) due to the presence of appreciable amounts of moldic and intragranular pores. In the absence of moldic pores, eogenetic cementation of the grainstones by equant, meteoric calcite, such as in HST of D3 resulted in extremely low porosity (< 3%) and nil permeability.

(2) Reservoir-quality enhancement has resulted from the dissolution of peloids, which is commonly accompanied with recrystallization, partial dolomitization and/or formation of equant calcite cement. Average porosities (moldic, intragranular and intercrystalline micro-porosity) are around 28% and permeability of ca. 285 mD. Slight to moderate dolomitization of the mudstones has often not resulted in a considerable improvement of porosity and permeability. The formation of large amounts of moldic porosity can be deceiving when viewed in density logs, but ultimately contributes little if any to reservoir permeability, and hence to oil recovery from the interval. However, permeability improvement may occur when the moldic pores are connected with the intercrystalline pores. (3) Reservoir-quality preservation, which resulted from partial cementation of the peloid grainstones (typical porosity ca. 30%; permeability ca. 750 mD) by scattered calcite cement (equant, syntaxial and isopachous grain rims) and rhombic dolomite. These cements have supported the framework of the limestones from extensive mechanical and chemical compaction (Purser, 1989; Tucker, 1993), particularly when the ductile peloids-rich composition of the limestones is considered. Grainstones cemented nearly exclusively by isopachous grain-rims calcite can on average have porosity of ca. 20% and permeability of ca. 1,000 mD. Variation in permeability among such peloid grainstones is presumably caused by variations in extent of pore-throat blockage by the scattered equant calcite and rhombic dolomite.

Linking Diagenesis to Sequence Stratigraphy

The spatial and temporal distribution of eogenetic alterations in Arab D and C members has been linked to the various systems tracts, which include the highstand systems tracts (HST), transgressive systems tracts (TST), and lowstand systems tracts (LST; or lowstand/ramp margin wedge LSW/RMW), and key sequence-stratigraphic surfaces, including the transgressive surface (TS), maximum flooding surface (MFS), sequence boundaries (SB), parasequence boundaries (PB), and parasequence set boundaries (PSB). A conceptual model for the distribution of diagenetic alterations *versus* sequence stratigraphy has been developed (Figure 19).

Diagenesis along PB, MFS, TS, PSB and within TST

Diagenesis along MFS and PSB, and within TST are presumably controlled by low rates of sedimentation relative to rates of rise in the relative sea level, i.e. long residence time of the sediments on the seafloor (Jervey, 1988; Loutit et al., 1988), which implies extensive marine pore-water diagenesis and marine bioturbation (Baum and Vail, 1988; Tucker, 1993; Morad et al., 2011). Typical diagenetic alterations encountered include dolomitization of mudstones, wackestones and packstones (Tucker, 1993). Dolomitization in the Arab D5–D3 occurs locally in limestone-dominated successions, whereas dolomitization is widespread throughout the Arab D2 and C, presumably denoting a trend of progressive, significant fall in the relative sea level, which would result in evaporative development of lagoonal brine (Figure 16). High frequency oscillation of relative sea level has presumably been encountered during the overall trend of fall in the relative sea level, which could account for the presence of interbedded limestones and dolostones in the Arab D2 and, particularly the Arab C (Figure 16).

The most prominent MFS on top of cycle D5 is covered by a 25 ft thick dolomitized zone, the lower part of which is characterized by extensive dolomitization of heavily bioturbated wackestones. The absence of sulfate deposits and intercrystalline cements suggests that dolomitization did not occur according to the evaporative models. Dolomitization along this MFS and along the PSB, which results in impermeable, laterally extensive dolostones, was probably accomplished by slightly modified marine pore waters (Poppe et al., 1990; Tucker, 1993; Sánchez-Román et al., 2009). Dolomitization was likely enhanced by long residence time of the sediments at the seafloor during marine transgression and by bioturbation (Wilkinson, 1991), which could facilitate dolomite nucleation by increasing carbonate alkalinity owing to aerobic and anaerobic decay of organic matter in bioturbation sites (Mazzulo et al., 1995; Bontognali et al., 2010). The tight, laterally extensive dolostones formed along PSB (e.g. along the top of sub-zones D4U, D3L, and D3M in a well to the north) may act as barriers or baffles for fluid flow, and hence cause reservoir compartmentalization. Extension of these PSB into the shoal facies is commonly marked by the formation of fairly porous and permeable grainstones. PSB in the Arab C, which were presumably formed during falls in the relative sea level and consequent isolation of the lagoon from open-marine environment (Sarg, 1988), are marked by the occurrence of sulfate beds, which can thus act as barriers for fluid flow over the entire inner ramp area. Dolomitization cannot be linked systematically to lower-order MFSs, which occur on top of the TST, in the Arab D4–D3. In some cases dolomitization is not encountered, whereas in other cases dolomitization varies from slight to extensive. The reason behind this variation is poorly understood, but could be related to the duration of marine transgression and extent of bioturbation (Tucker, 1993; Morad et al., 2011). In most Arab D4 and D3 intervals, the TSTs are considerably thinner than the HSTs, and are commonly characterized by moderate to extensive dolomitization and dolomite cementation. Selective dolomitization is restricted to bioturbation sites, which probably played a role in dolomitization (Tucker, 1993; Morad et al., 2011).

PS-6 to PS-10 in the Arab C and D2 display shallowing upward cycles culminated with anhydrite layer. PS-6 of the Arab D2 consists of dolostone with fenestral pores filled by anhydrite cement. PS-7 to PS-10 of the Arab C consists of cycles of dolopackstones/dolograinstones, which are capped by anhydrite layers. An upward increase in dolomitization, dolomite cementation, and anhydrite cementation within each of these PS are suggested to have occurred during high-frequency changes in the relative sea level (upward decrease) and concomitant progressive isolation of the lagoon from open-marine environment (Sarg, 1988). Transgression events and formation of PSB after deposition of

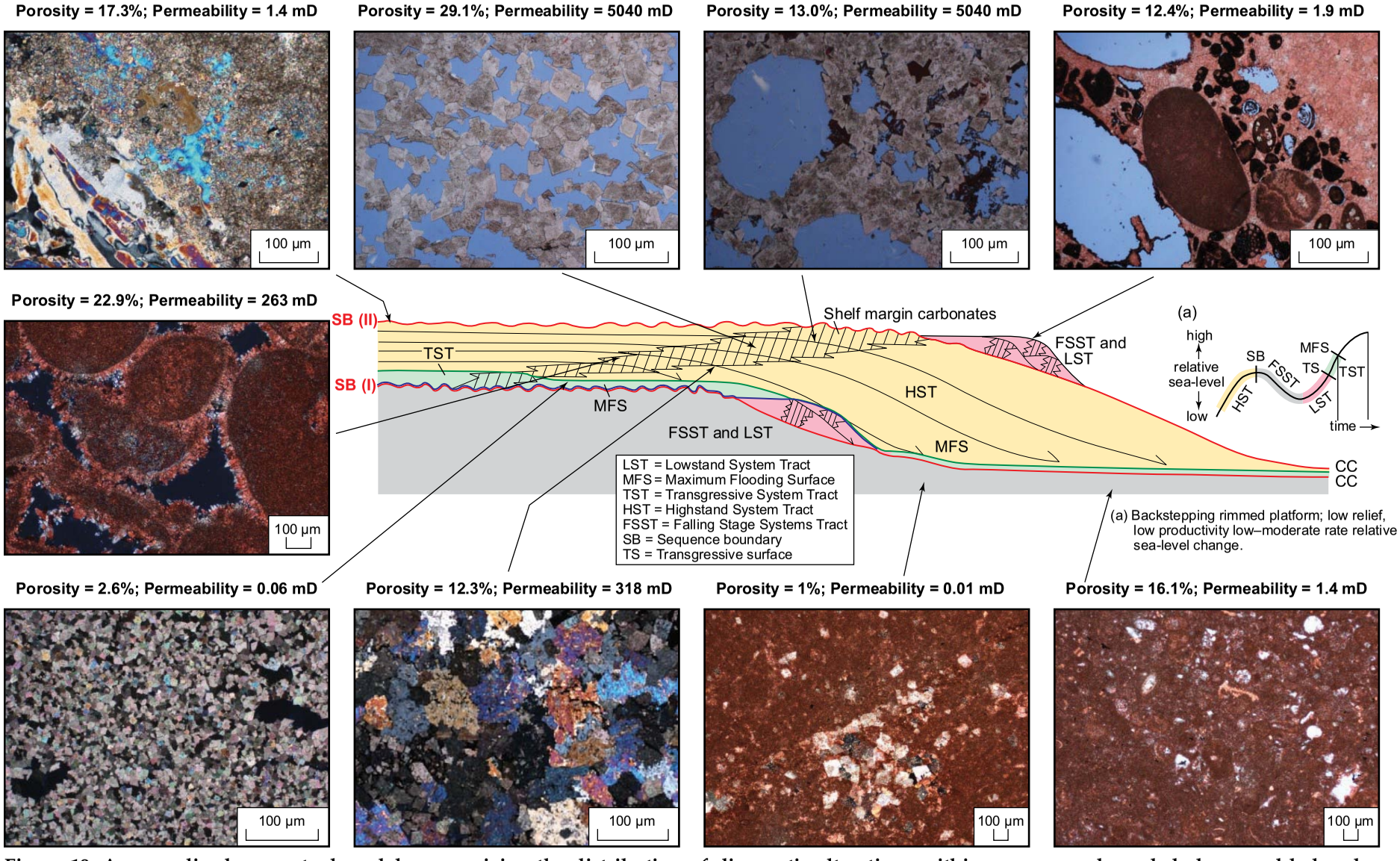

Figure 19: A generalized conceptual model summarizing the distribution of diagenetic alterations within a sequence bounded above and below by surfaces of subaerial exposure (i.e. sequence boundaries, SB) in the Arab Formation. The alterations are shown in the various systems tracts and along key sequence-stratigraphic surfaces. Meteoric water percolation below the SB results in the formation of abundant moldic porosity in the lowstand wedge (LSW) rudstones. It should be noted that dolomitization and cementation by intercrystalline sulfate cements are much more extensive in the Arab D2 and C than in the Arab D5–D3. The latter are characterized instead by more frequent limestone occurrence with no or locally variable extents of dolomitization and large amounts of calcite cement (isopachous, syntaxial overgrowths and equant blocky). (Figure modified after Bosence and Wilson, 2003).

each PS was not accompanied by percolation of seawater below these marine flooding surfaces owing to the presence of the impermeable anhydrite caps. This postulation is, thus, further indicating that dolomitization below the PSB of PS-6 to PS-10 occurred by the sabkha and seepage reflux models.

Diagenesis along SB, HST and LSW

Diagenesis along the SB and within the HST and LSW (or RMW) typically reflects conditions related to higher rates of sedimentation than rates of rise in the relative sea level (Sarg, 1988). These conditions are commonly associated with the flux of meteoric waters (Tucker, 1993; Morad et al., 2011). However, the SB is commonly amalgamated by TS, and hence coincides with a shift from meteoric to marine pore waters (Morad et al., 2011). The most common eogenetic alterations, which are encountered below the SB and within the HST and, particularly, the LSW include grain dissolution and cementation by dominantly equant blocky calcite. Subsequently, circulation of the lagoonal brines has presumably caused dolomitization and dolomite cementation of the grainstones (Machel, 1986; Morrow, 2001; Jones and Xiao, 2005). Similar to the TST limestones of the Arab D, the presence of scattered dolomite and equant blocky, isopachous and/or syntaxial calcite overgrowths have supported the framework of HST limestones, and thus prevented substantial compaction and destruction of intergranular porosity. Dolomitiztion of some of the grainstones, particularly in the HSTs of D4–D2 and C, has resulted in the formation of abundant, coarse-crystalline dolomite, probably denoting the intial high permeability of these sediments (Al-Aasm, 2000).

SUMMARY MODEL FOR RESERVOIR QUALITY EVOLUTION

Reservoir quality and heterogeneity distribution and evolution in the D and C members of the Arab Formation are controlled profoundly by the spatial and temporal distribution of diagenetic alterations. These alterations are in turn controlled by the arid paleo-climatic conditions, depositional facies, and the sequence-stratigraphic framework, which were developed during a second-order regression segment of a supersequence. The supersequence is composed of four third-order shallowing upward sequences deposited across a distally steepened ramp characterized by a lagoon, an offshore break caused by the presence of barrier islands, and a slope. Changes in the relative sea level exerted a major control on the chemical composition of the lagoon water; a fall in the relative sea level would have resulted in semi- to complete isolation of the lagoon from the open sea, implying evaporative increase in the salinity (and density) of the lagoon water, which led to the formation of brines. These dense brines could circulate and induce eogenetic dolomitization to earlier deposited HST and TST subtidal lagoon packstones and shoal grainstones/rudstones, and LSW grainstones and rudstones according to the seepage reflux dolomitization model (Machel, 1986; Morrow, 2001; Jones and Xiao, 2005). Contemporaneously, pore waters in the peritidal mud flat were subjected to evaporative increase in salinity and density to sink into these sediments (Tucker and Wright, 1990). Typical diagenetic alterations include the formation of anhydrite/gypsum nodules, which results in an increase of Mg^{2+}/Ca^{2+} activity ratio in the pore waters, and hence dolomitization of the lime mud deposits according to the sabkha model. These dolomitization events and concomitant sulfate cementation of dolostones across the inner ramp influenced mainly the upper parts of the highstand systems tracts (HST) of primarily the Arab D2 and C, which were deposited under conditions of overall sea-level lowstand being subjected to high-frequency (fourth- and fifth-order) changes in relative sea level (Sarg, 1988). The overall upward decrease in crystal size of dolostones in the Arab D2 and C coupled with an increase in anhydrite and gypsum cements account for the general upwards decrease in reservoir porosity from PS-1 to PS-10.

The TST deposited in the outer ramps (mudstones, wackestones, and packstones) were subjected to neomorphism, stylolitization, as well as eogenetic marine calcite cementation and limited dolomitization. Extensive dolomitization occurred, instead, about the PSB, MFS and in the early HST sediments. Dolomitization of these sediments, which is also encountered in the TST (particularly along the MFS) of the inner ramp mudstones and wackestones, lacks associated sulfate cements accompanying the evaporative dolomitization (i.e. the sabkha and seepage reflux models). Dolomitization in the TST, particularly along MFS, is suggested to be promoted by an increase in carbonate alkalinity in suboxic to anoxic pore waters caused by anaerobic and aerobic bacterial decay of locally abundant organic-matter concentration within bioturbation sites (e.g. Mazzullo et al., 1995; Vasconcelos and McKenzie, 1997; Sánchez-Román et al., 2008). Initial nucleation of dolomite in these

sediments would have resulted in establishment of a chemical gradient along which diffusion of Mg^{2+}, Ca^{2+}, and dissolved carbon occurred into the pore waters from overlying seawater. Extensive dolomitization, which resulted in fine-crystalline, tightly interlocked dolostones, was likely promoted by low sedimentation rates in the TST, particularly below the MFS. These dolostones can act as diagenetic baffles or seals for fluid flow, and hence induce reservoir compartmentalization (Tucker, 1993; Morad et al., 2011).

The TST and HST grainstones and packstones deposited during episodes of sea-level highstand under open-marine conditions (i.e. in the outer rim or during sea-level rise in the back-shoal and lagoon) are slightly to extensively dolomitized. In these limestones, coarse-crystalline rhombic dolomite replaces the grains and fills the intergranular and moldic pores. The TST limestones, which are finer grained than HST limestones, contain smaller amounts of calcite cement and moldic/intragranular pores, denoting their low depositional permeability, and hence smaller rates of fluid flow. The presence of scattered rhombic dolomite, syntaxial calcite overgrowths, equant calcite crystals, and isopachous calcite in peloidal grainstones has helped preserve reservoir quality through prevention of extensive chemical and mechanical compaction. However, the scattered equant calcite and rhombic dolomite locally block the pore throats, thus causing variable extents of permeability deterioration in the grainstones.

Deposition of the permeable LST grainstones/rudstones on the fore-shoal due to fall in the relative sea level results in meteoric-water percolation below SB, which results in pervasive grain (presumably aragonite bioclasts) dissolution and formation of abundant moldic porosity as well as cementation by equant (in some cases drusy) low-Mg calcite due to percolation of meteoric waters below surfaces of subaerial exposure. Isolation of the lagoon and development of brines by evaporation of seawater has presumably resulted in dolomitization of the grainstones according to the seepage reflux model. The isolated moldic pores have resulted in drastic permeability deterioration in many of the grainstones and dolograinstones.

The above described eogenetic dolomites have been subjected to various extents of recrystallization concomitant with the precipitation of a new dolomite generation during mesodiagenesis. Many of the grainstones and dolograinstones have also been subjected to cementation by coarse-crystalline, rarely saddle-shaped, rhombic dolomite crystals during mesodiagenesis as suggested by the high homogenization temperatures and fluid salinities as well as low $\delta^{18}O_{VPDB}$ values. Cementation by small amounts of moldic pore-filling, dolomite-replacing quartz crystals (average T_h = ca. 100°C) occurred locally. It has been argued by several authors (e.g. Heasley et al., 2000) that carbonate reservoirs remain partially water-wet during slow and incomplete oil emplacement, particularly in micro-porosity rich rocks. Hence, diagenetic processes (e.g. recrystallization), which are mediated by diffusion may continue, yet at reduced rates, subsequence to oil charging into the reservoirs. Later diagenetic events in the dolograinstones include: (1) cementation by anhydrite and gypsum; (2) dissolution of these sulfate cements, which resulted in considerable reservoir-quality improvement. The timing and mechanisms of sulfate cement dissolution are poorly constrained, but may have been caused by thermal sulfate reduction; (3) the main phase of oil charging into the reservoirs; and (4) the precipitation of blocky anhydrite and gypsum in fractures associated with faults during oil migration, representing the last important cement in the Arab D and C.

CONCLUSIONS

- Dolomitization in the Arab Formation occurred mostly during eodiagenesis by: (1) seepage reflux of evaporative brines into earlier deposited highstand (HST) and transgressive (TST) subtidal packstones and shoal grainstones/rudstones, as well as lowstand wedge (LSW) grainstones and rudstones; and (2) sabkha evaporative dolomitization of peritidal mudstone, and microbially mediated dolomitization in bioturbated subtidal mudstones along surfaces of marine transgression. Dolomitization of grainstones/rudstones, which was most extensive in parasequence sets of the Arab C, was accompanied by the formation of abundant intercrystalline and moldic pores, which have been filled by gypsum and anhydrite cements (T_h ca. 95–105°C; salinity ca. 16–22 wt% NaCl equivalent).

- Examination of fluid inclusions by fluorescence microscopy revealed that oil charging into the reservoir occurred during formation of two major phases: (1) coarse-crystalline dolomite formed by recrystallisation of previous fine-crystalline dolomites, and (2) fracture-filling anhydrite and gypsum, which represent the last cement generation (possibly still ongoing) in the Arab Formation.
- Reservoir quality in the limestones of the Arab D4 and D3 members was controlled by: (1) porosity creation owing to dissolution of the bioclasts; and (2) porosity preservation due to the presence of isopachous calcite rims around the peloids, syntaxial calcite overgrowths around crinoids, and scattered crystals of equant calcite and rhombic dolomite, which prevented pervasive compaction.
- The key parameters, which control the reservoir quality in Arab D2 and Arab C, include: (1) upward increase in dolomitization and anhydrite cementation within parasequence sets and the formation of the anhydrite cap; and (2) extent of dissolution of anhydrite/gypsum cement that filled the intercrystalline and moldic pores.
- The origin of fluids that caused dissolution of anhydrite and gypsum cements and concomitant formation of late diagenetic calcite cement, are poorly constrained, but could be related to thermal sulfate reduction.
- Distribution of early diagenetic alteration is constrained within the context of sequence stratigraphy, both of which are strongly controlled by changes in the relative sea level. The main features that link diagenesis to sequence stratigraphy include: (1) formation of eogenetic equant calcite and abundant moldic porosity owing to grain dissolution occuring mainly in grainstones and rudstones of the lowstand wedge (LSW), which was deposited in the fore-shoal during major falls in the relative sea level and/or subaerial shoal exposures (i.e. below sequence boundaries). (2) Dolomitization by evaporative brines has switched on and off by high-frequency, relative sea-level changes during deposition of the Arab D2 and C. Upward increase in dolomitization and anhydrite cementation in these units is accompanied by a gradual upward decrease in permeability. Each parasequence set is capped by an anhydrite layer, which induces compartmentalization in this reservoir interval. (3) Dolomitization within the transgressive systems tracts of the Arab D4 and D3, particularly along marine transgressive surfaces and parasequence set boundaries, is suggested to have been mediated by bioturbation (which may have increased carbonate alkalinity) and diffusion of dissolved Ca, Mg and C from the overlying seawater along chemical gradient established with the pore waters.

ACKNOWLEDGEMENTS

We thank the Oil Subcommittee of Abu Dhabi National Oil Company (ADNOC) for permission to conduct and publish this research work. We thank Marwan Haggag for the excellent coordination of the research collaboration between the Petroleum Institute of Abu Dhabi and ADNOC and its operating companies. We are grateful to Mohamed Elhami of the Abu Dhabi Offshore Exploration Company (ADMA-OPCO) for discussions and for providing us with necessary material and data. Constructive review of the manuscript by two anonymous GeoArabia referees is gratefully acknowledged. The authors thank GeoArabia Designer, Nestor "Niño" Buhay IV, for designing the paper for press.

REFERENCES

Adams, J.E. and M.L. Rhodes 1960. Dolomitization by seepage refluxion**.** American Association of Petroleum Geologists Bulletin, v. 44, p. 1912-1920.

ADMA-OPCO Team Study 1998. Arab C and D. Integrated Multidisciplinary Reservoir Characterisation Study. Abu Dhabi, Confidential Report.

Al-Aasm, I.S., B.E. Taylor and B. South 1990. Stable isotope analysis of multiple carbonate samples using selective acid extraction. Chemical Geology, v. 80, p. 19-125

Al-Aasm, I.S. 2000. Chemical and isotopic constraints for recrystallization of sedimentary dolomites from the Western Canada Basin. Aquatic Geochemistry, v. 6, p. 227-248.

Al-Suwaidi, A. and S.K. Aziz 1998. Regional basin modelling: an approach to understand shelfal carbonate reservoirs of the Oxfordian and Kimmeridgian in offshore Abu Dhabi. Society of Petroleum Engineers, SPE Paper 49471, p. 148-158.

Al-Suwaidi, A. and S.K. Aziz 2002. Sequence stratigraphy of Oxfordian and Kimmeridgian shelf carbonate reservoirs, offshore Abu Dhabi. GeoArabia, v. 7, no. 1, p. 31-44.

Ali, M.Y. and A.B. Watts 2009. Subsidence history, gravity anomalies and flexure of the United Arab Emirates (UAE) foreland basin. GeoArabia, v. 14, no. 2, p. 17-44.

Azer, S.R. and R.G. Peebles, 1995. Sequence stratigraphy of the Hith/Upper Arab Formation, offshore Abu Dhabi, U.A.E. Proceedings of the 9th Middle East Oil Show, SPE 29799, p. 277-292.

Azer, S. and R.G. Peebles 1998. Sequence stratigraphy of the Arab A and C members and Hith Formation, offshore Abu Dhabi. GeoArabia, v. 3, no. 2, p. 251-268.

Baker, B.A. and M. Kastner 1981. Constraints on the formation of sedimentary dolomite**.** Science, v. 213, p. 215-216.

Barclay, S.A. and R.H. Worden 2000. Effects of reservoir wettability on quartz cementation in oil fields. In R.H. Worden and S. Morad (Eds.), Quartz Cementation of Sandstones. Blackwell Science, Oxford, International Association of Sedimentologists (IAS) Special Publication no. 29, p. 103-118.

Baum, G. and P.R. Vail 1988. Sequence stratigraphic concepts applied to Paleocene outcrops, Gulf and Atlantic basins. In C.K. Wilgus, B.S. Hastings, C.G.C. Kendall, H.W. Posamentier, C.A. Ross and J.C. Van Wagoner (Eds.), Sea-level Changes: an Integrated Approach. Society of Economic Paleontologists and Mineralogists, Special Publication, v. 42, p. 310-327.

Beydoun, Z.R. 1991. Arabian Plate Hydrocarbon Geology and Potential- A Plate Tectonic Approach. American Association of Petroleum Geologists, Studies in geology no. 33.

Bodnar, R.J. 1992. Revised equation and table for freezing point depressions of H_2O-salt fluid inclusions Inclusions, Program and Abstracts, Lake Arrowhead, CA, v. 14, p. 15.

Bontognali, T.R.R., C. Vasconcelos, R.J. Warthmann, S.M. Bernasconi, C. Dupraz, C.J. Strohmenger and J.A. McKenzie 2010. Dolomite formation within microbial mats in the coastal sabkha of Abu Dhabi (United Arab Emirates). Sedimentology, v. 57, p. 824-844.

Bosence, D.W.J. and C.L. Wilson 2003. Sequence stratigraphy of carbonate depositional systems. In A.L. Coe (Ed.), The sedimentary record of sea-level change. Cambridge University Press, p. 234-256.

Bourque, P-A., M.M. Savard, G. Chi and P. Dansereau 2001. Diagenesis and porosity evolution of the Upper Silurian–lowermost Devonian West Point reef limestone, eastern Gaspé Belt, Québec Appalachians**.** Bulletin of Canadian Petroleum Geology, v. 94, p**.** 299-326.

Bush, P. 1973. Some Aspects of the Diagenetic History of the Sabkha in Abu Dhabi, Persian Gulf. In The Persian Gulf. Springer-Verlag, New York, p. 395-407.

Cantrell, D.L., A. Al-Khammash and P.D. Jenden 2007. Characterization and significance of dedolomite in Wadi Nisah, central Saudi Arabia. GeoArabia, v. 12, no. 3, p. 15-30.

Caron, V., C.S. Nelson and P.J.J. Kamp 2005. Sequence stratigraphic context of syndepositional diagenesis in cool-water shelf carbonates: Pliocene limestones, New Zealand**.** Journal of Sedimentary Research, v. 75**,** p. 231-250.

Choquette, P.W. and N.P. James 1987. Diagenesis # 12. Diagenesis in Limestones-3. The deep burial environment. Geoscience Canada, v. 14, p. 3-35.

Choquette, P.W., and E.E. Hiatt 2008. Shallow-burial dolomite cement: A major component of many ancient sucrosic dolomites. Sedimentology, v. 55, p. 423-460.

Choquette, P.W. and L.C. Pray 1970. Geologic nomenclature and classification of porosity in sedimentary carbonates. American Association of Petroleum Geologists Bulletin, v. 54, p. 207-250.

De Matos, J.E. and R.F. Hulstrand 1995. Regional characteristics and depositional sequences of the Oxfordian and Kimmeridgian, Abu Dhabi. In M.I. Al-Husseini (Ed.), Middle East Petroleum Geosciences, GEO94, Gulf PetroLink, Bahrain, v. 1, p. 346-356.

Eberli, G.P., F.S. Anselmetti, J.A.M. Kenter, D.F. McNeill and L.A. Melim 2001. Calibration of seismic sequence stratigraphy with cores and logs (*in* Subsurface geology of a prograding carbonate platform margin, Great Bahama Bank; results of the Bahamas Drilling Project, Ginsburg). Special Publication - Society for Sedimentary Geology, v. 70, p. 241-265.

Egeberg, P.K. and P. Aagaard 1989. Origin and evolution of formation waters from oil fields on the Norwegian shelf. Applied Geochemistry, v. 4, p. 131-142.

Esrafili-Dizaji, B. and H. Rahimpour-Bonab 2009. Effects of depositional and diagenetic characteristics on carbonate reservoir quality: a case study from the South Pars gas field in the Persian Gulf Petroleum Geoscience, v. 15, p. 325-344.

Esteban, M. and C. Taberner 2003. Secondary porosity development during late burial in carbonate reservoirs as a result mixing and/or cooling of brines (*in* Proceedings of Geofluids IV). Journal of Geochemical Exploration, v. 78-79, p. 355-359.

Friedman, I. and J.R. O'Neil 1977. Compilation of stable isotopic fractionation factors of geochemical interest. In M. Fleischer (Ed.), Data of Geochemistry. United States Geological Survey Professional Paper, 440-KK, 6th edition, 12 p.

Froelich, P.N., G.P. Klinkhammer, M.L. Bender, N.A. Luedtke, G.R. Heath, D. Cullen, P. Dauphin, D. Hammond, B. Hartman and V. Maynard 1979. Early oxidation of organic matter in pelagic sediments of the eastern equatorial Atlantic: suboxic diagenesis. Geochimica et Cosmochimica Acta, v. 43, p. 1075-1090.

Gill, I., C. Moore and P. Aharon 1995. Evaporitic mixed-water dolomitization on St. Croix, U.S.V.I. Journal of Sedimentary Research, v. A65, p. 591-604.

Glumac, B. and K.R. Walker 2002. Effects of Grand-Cycle Cessation on the Diagenesis of Upper Cambrian Carbonate Deposits in the Southern Appalachians, U.S.A. Journal of Sedimentary Research, v. 72, p. 570-586.

Goldhammer, R.K., P.A. Dunn and I.A. Hardie 1990. Depositional cycles, composite sea-level changes, cycle stacking patterns, and the hierarchy of stratigraphic forcing: Examples from Alpine Triassic platform carbonates. Geological Society of America Bulletin, v. 102, p. 535-562.

Goldstein, R. H. 2001. Fluid inclusions in sedimentary and diagenetic systems. Lithos, v. 55, p. 159-193.

Goldstein, R. H. and T.J. Reynolds 1994. Systematics of Fluid inclusions in Diagenetic Minerals. SEPM Short Course 31, 199 p.

Harris, P.M. 2010. Delineating and quantifying depositional facies patterns in carbonate reservoirs: Insight from modern analogs. American Association of Petroleum Geologists Bulletin, v. 94, p. 61-86.

Heasley, E.G., R.H. Worden and J.P. Hendry 2000. Cement distribution in a carbonate reservoir: recognition of a palaeo oil-water contact and its relationship to reservoir quality in the Humbly Grove Field, onshore, UK. Marine and Petroleum Geology, v. 17, p. 639-654.

Jervey, M.T. 1988. Quantitative geological modeling of siliciclastic rock sequences and their seismic expression. In C.K. Wilgus, B.S. Hastings, C.G.C. Kendall, H.W. Posamentier, C.A. Ross and J.C. Van Wagoner (Eds.), Sea-level Changes: an Integrated Approach. Society of Economic Paleontologists and Mineralogists, Special Publication, v. 42, p. 47-69.

Jones, J.D. and Y. Xiao 2005. Dolomitization, anhydrite cementation, and porosity evolution in a reflux system: Insights from reactive transport models. American Association of Petroleum Geologists Bulletin, v. 89, p. 577-601.

Jones, G.D., F.F. Whitaker, P.L. Smart and W.E. Sanford 2003. Fate of reflux brines in carbonate platforms. Geology, v. 30, p. 371-374.

Kaufman, J. 1994. Numerical models of fluid flow in carbonate platforms; implications for dolomitization. Journal of Sedimentary Research, v. 64, p. 128-139.

Kupecz, J.A. and L.S. Land 1991. Late-stage dolomitization of the Lower Ordovician llenburger Group, West Texas. Journal of Sedimentary Research, v. 61, p. 551-574.

Land, L.S. 1983. The application of stable isotopes to studies of the origin of dolomite and to problems of diagenesis of clastic sediments. In M.A. Arthur, T.F. Anderson, I.R. Kaplan, J. Veizer and L.S. Land (Eds.), Stable Isotopes in Sedimentary Geology. Society of Economic Paleontologists and Mineralogists Short Course Note 10, pp. 4.1-4.22.

Le Nindre, Y.M., J. Manivit, H. Manivit and D. Vaslet 1990. Stratigraphie sequentielle du Jurassique et du Cretace en Arabie Saoudite. Bulletin de la Societe Geologique de France, v. 6, p. 1025-1034

Loucks, R.G. and J.F. Sarg 1993. Carbonate Sequence Stratigraphy, Recent development and applications. American Association of Petroleum Geologists Memoir 57, 545 p.

Loutit, T.S., J. Hardenbol and P.R. Vail 1988. Condensed sections: the key to age determination and correlation of continental margin sequences. In C.K. Wilgus, B.S. Hastings, C.G.C. Kendall, H.W. Posamentier, C.A. Ross and J.C. Van Wagoner (Eds.), Sea-level Changes: an Integrated Approach. Society of Economic Paleontologists and Mineralogists, Special Publication, v. 42, p. 183-213.

Machel, H.G. 1986. Early lithification, dolomitization, and anhydritization of Upper Devonian Nisku buildups, subsurface of Alberta, Canada. In J.H. Scroeder and B.H. Purser (Eds.), Reef Diagenesis, Springer Verlag, Berlin, p. 336-356.

Machel, H.G. 1987. Some aspects of diagenetic sulphate-hydrocarbon redox reactions. In J.D. Marshall (Ed.), Diagenesis of sedimentary sequences. Geological Society of London Special Publication no. 36, p. 15-28.

Machel, H.G., P.A. Cavell and K.S. Patey 1996. Isotopic evidence for carbonate cementation and recrystallization, and for tectonic expulsion of fluids into the Western Canada Sedimentary Basin. Geological Society of America Bulletin, v. 108, p. 1108-1119.

Machel, H.G. and H. Hubscher 2000. The Devonian Grosmont heavy oil reservoir in Alberta, Canada. Zentralblatt fur Geologie und Palaontologie, Teil I, Heft 1/2, p. 55-84.

Machel, H.G. 2004. Concepts and models of dolomitization: a critical reappraisal. In C.J.R. Braithwaite, C. Rizzi and G. Darke (Eds.), The Geometry and Petogenesis of Dolomite Hydrocarbon Reservoirs. Geological Society of London Special Publication, no. 235, p. 7-63.

Machel, H.G. and B.E. Buschkuehle 2008. Diagenesis of the Devonian Southesk-Cairn Carbonate Complex, Alberta: Marine cementation, burial dolomitization, thermochemical sulfate reduction, and squeegee fluid flow. Journal of Sedimentary Research, v. 78, p. 366-389.

Maiklem, W.R., D.G. Bebout and R.P. Glaister 1969. Classification of anhydrite; a practical approach. Bulletin of Canadian Petroleum Geology, v. 17, p. 194-233.

Malone, M.J., P.A. Baker and S.J. Burns 1994. Recrystallization of dolomite: evidence from the Monterey Formation (Miocene) California. Sedimentology, v. 41, p. 1223-1239.

Mazzullo, S.J. 1992. Geochemical and neomorphic alteration of dolomite: a review: Carbonates and Evaporites, v. 7, p. 21-37.

Mazzullo, S.J., W.D. Bischoff and C.S. Teal 1995. Holocene shallow-subtidal dolomitization by near-normal seawater, northern Belize. Geology, v. 23, p. 341-344.

Mazzullo, S.J. 2000. Organogenic dolomitization in peritidal to deep sea sediments. Journal of Sedimentary Research, v. 70, p. 10-23.

McLimans, R.K. 1987. The application of fluid inclusions to migration of oil and diagenesis in petroleum reservoirs. In J.S. Hanor, Y.K. Kharaka and L.S. Land, conveners, Geochemistry of waters in deep sedimentary basins; selected contributions from the Penrose conference. Applied Geochemistry, v. 2, p. 585-603.

Meyers, W.J., F.H. Lu and J. Zackariah 1997. Dolomitization by mixed evaporative brines and freshwater, late Miocene carbonates, Nijar, Spain. Journal Sedimentary Petrology, v. 67, p. 898-912.

Moore, C.H. 2001. Carbonate Reservoirs, Porosity Evolution and Diagenesis in a Sequence Stratigraphic Framework. Development in Sedimentology, v. 55, Amsterdam, Elsevier, 444 p.

Morad, S. 1998. Carbonate cementation in sandstones: distribution patterns and geochemical evolution, In S. Morad (Ed.), Carbonate Cementation in Sandstones. Blackwell Science, Oxford, International Association of Sedimentologists (IAS) Special Publication no. 26, p. 1-26.

Morad, S., J.M. Ketzer and L.F. De Ros 2000. Spatial and temporal distribution of diagenetic alterations in siliciclastic rocks: implications for mass transfer in sedimentary basins. Sedimentology, v. 47, p. 95-120.

Morad, S., J.M. Ketzer and L.F. De Ros 2011. Linking diagenesis to sequence stratigraphy: integrated tool for deciphering and predicting reservoir quality distribution. In S. Morad, J.M. Ketzer and L.F. De Ros (Eds.), Linking Diagenesis to Sequence Stratigraphy in Sedimentary Successions. Blackwell Science, Oxford International Association of Sedimentologists (IAS) Special Publication.

Moss, S. and M.E. Tucker 1995. Diagenesis of Barremian-Aptian platform carbonates (the Urgonian Limestone Formation of SE France): near-surface and shallow-burial diagenesis. Sedimentology, v. 42, p. 853-874.

Morrow, D.W. and B.D. Ricketts 1988. Experimental investigation of sulfate inhibition of dolomite and its mineral analogues. In V. Shukla and P.A. Baker (Eds.), Sedimentology and Geochemistry of Dolostones. Society of Economic Paleontologists and Mineralogists, Special Publication, v. 43, p. 25-39.

Morrow, D.W. 2001. Distribution of Porosity and Permeability in Platform Dolomites: Insight from the Permian of West Texas: Discussion. American Association of Petroleum Geologists Bulletin, v. 85, p. 525-529.

Mountjoy, E.W. and J.E. Amthor 1994. Has burial dolomitization come of age? Some answers from the eastern Canadian Sedimentary Basin. In B. Purser, M. Tucker, D. Zenger (Eds.), Dolomites. A volume in Honour of Dolomieu. International Association of Sedimentologists, Special Publication, v. 21, p. 203-229.

Nader, F.H., R. Swennen and E. Keppens 2008. Calcitization/dedolomitization of Jurassic dolostones Lebanon): results from petrographic and sequential geochemical analyses. Sedimentology, v. 55, p. 1467-1485.

Neuweiler, F., V. d'Orazio, A. Immenhauser, G. Geipel, K.-H. Heise, C. Cocozza, T.M. Miano 2003. Fulvic acid-like organic compounds control nucleation of marine calcite under suboxic conditions. Geology, v. 31, p. 681-684.

Poppe, L.J., R.C. Circe and A.K. Vuletich 1990. A dolomitized shelfedge hardground in the northern Gulf of Mexico. Sedimentary Geology, v. 66, p. 29-44.

Purser, B. H. 1989. Early diagenesis and the preservation of porosity in Jurassic limestones. Journal of Petroleum Geology, v. 1, p. 83-94.

Saller, A.H. and N. Henderson 2001. Distribution of Porosity and Permeability in Platform Dolomites: Insight from the Permian of West Texas: Reply. American Association of Petroleum Geologists Bulletin, v. 85, p. 530-532.

Sánchez-Román, M., C. Vasconcelos, T. Schmid, T. Dittrich, J.A. McKenzie, R. Zenobi and M.A. Rivadeneyra 2008. Aerobic microbial dolomite at the nanometer scale: Implications for the geologic record**.** Geology, v. 36, p. 879-882.

Sánchez-Román, M., J.A. McKenzie, A. Rebello Wagener, M.A. Rivadeneyra and C. Vasconcelos 2009. Presence of sulfate does not inhibit low-temperature dolomite precipitation. Earth and Planetary Science Letters, v. 285, p. 131-139.

Sarg, J.F. 1988. Carbonate sequence stratigraphy. In C.K. Wilgus, B.S. Hastings, C.G.St.C. Kendall, H.W. Posamentier, C.A. Ross and J.C. Van Wagoner (Eds.), Sea-Level Changes: an Integrated Approach. Society of Economic Paleontologists and Mineralogists, Special Publication, v. 42, p. 155-181.

Sibley, D.F. and J.M. Gregg 1987. Classification of dolomite rock textures. Journal of Sedimentary Petrology, v. 57, p. 967-975.

Slaughter, M. and R.J. Hill 1991. The influence of organic matter in organogenic dolomitization. Journal of Sedimentary Research, v. 61, p. 296-303.

Smith, L.B., G.P. Eberli and M. Sonnenfeld 2004. Sequence-stratigraphic and paleogeographic distribution of reservoir-quality dolomite, Madison Formation, Wyoming and Montana, in Integration of Outcrop and Modern Analogs in Reservoir Modeling. American Association of Petroleum Geologists Memoir, v. 80, p. 67-92.

Stoessel, R.K. and C.H. Moore 1983. Chemical constraints and origins of four groups of Gulf Coast reservoir fluids. American Association of Petroleum Geologists Bulletin, v. 67, p. 896-906.

Swart, P.K., D.L. Cantrell, H. Westphal, C.R. Handford and C.G. Kendall 2005. Origin of Dolomite in the Arab-D Reservoir from the Ghawar Field, Saudi Arabia: Evidence from Petrographic and Geochemical Constraints. Journal of Sedimentary Research, v. 75, p. 476-491.

Tucker, M.E. and V.P. Wright 1990. Carbonate Sedimentology. Oxford, Blackwell Scientific Publications, 482 p.

Tucker, M.E. 1993. Carbonate Diagenesis and Sequence Stratigraphy. In V.P. Wright (Ed.), Sedimentology Review, Oxford, Blackwell Scientific Publications, v. 1, p. 51-72.

Tucker, M.E. and J. Booler 2002. Distribution and geometry of facies and early diagenesis: the key to accomodation space variations and sequence stratigraphy: Upper Cretaceous Congost Carbonate platform, Spanish Pyrinees. Sedimentary Geology, v. 146, p. 225-247.

Varol, B. and M. Magaritz 1992. Dolomitization, time boundaries and unconformities: examples from the dolostone of the Taurus Mesozoic sequence, south-central Turkey. Sedimentary Geology, v. 76, p. 117-133.

Vasconcelos, C. and J.A. McKenzie 1997. Microbial mediation of modern dolomite precipitation and diagenesis under anoxic conditions (Lagoa Vermelha, Rio de Janeiro, Brazil). Journal of Sedimentary Research, v. 67, p. 378-390.

Veizer, J., D. Ala, K. Azmy, P. Bruckschen, D. Buhl, F. Bruhn, G.A.F. Carden, A. Diener, S. Ebneth, Y. Godderis, T. Jasper, C. Korte, F. Pawellek, O.G. Podlaha and H. Strauss 1999. $^{87}Sr/^{86}Sr$, $\delta^{13}C$ and $\delta^{18}O$ evolution of Phanerozoic sea water. Chemical Geology, v. 161, p. 59-88.

Wang, B., and I.S. Al-Aasm 2002. Karst-controlled diagenesis and reservoir development: example from the Ordovician Main-reservoir carbonate rocks on the eastern margin of Ordos Basin, China: American Association of Petroleum Geologists Bulletin, v. 86, p. 1639-1658.

Warren, J. 2000. Dolomite; occurrence, evolution and economically important associations. Earth-Science Reviews, v. 52, p. 1-81.

Westphal, H., G.P. Eberli, L.B. Smith, G.M. Grammer and J. Kislak 2004. Reservoir characterization of the Mississippian Madison Formation, Wind River basin, Wyoming. American Association of Petroleum Geologists Bulletin, v. 88, p. 405-432.

Wierzbicki, R., J.J. Dravis, I.S. Al-Aasm and N. Harland 2006. Burial dolomitization and dissolution of Upper Jurassic Abenaki platform carbonates, Deep Panuke reservoir, Nova Scotia, Canada. American Association of Petroleum Geologists Bulletin, v. 90, p. 1843-1861.

Wilkinson, M. 1991. The concretions of the Bearreraig Sandstone Formation: geometry and geochemistry. Sedimentology, v. 38, p. 899-912.

Worden, R.H. and P.C. Smalley 1996. H_2S-producing reactions in deep carbonate gas reservoirs: Khuff Formation, Abu Dhabi. Chemical Geology, v. 133, p. 157-171.

Worden, R.H., P.C. Smalley and N.H. Oxtoby 1996. The effects of thermochemical sulfate reduction upon formation water salinity and oxygen isotopes in carbonate gas reservoirs. Geochimica et Cosmochimica Acta, v. 60, p. 3925-3931.

ABOUT THE AUTHORS

Sadoon Morad *has received BSc (1974) and MSc (1977) degrees in Geology from the University of Baghdad, Iraq and PhD (1983) degree in sedimentary petrology from Uppsala University, Sweden. He has published over 90 journal papers in the field of diagenesis. His main field of research is linking the impact of diagenesis on reservoir quality distribution to sequence stratigraphy, depositional facies, and burial-thermal history of siliciclastic and carbonate successions. He is based in the Department of Earth Sciences, Uppsala University and joined the Petroleum Institute of Abu Dhabi in 2007, where he is holding an ADOC (Abu Dhabi Oil Company) Chair Professor position*

smorad@pi.ac.ae

Ihsan Al-Aasm *earned his BSc (1974) and MSc (1977) degrees from the University of Baghdad, Iraq and his PhD from the University of Ottawa, Canada (1985). He worked at the Geological Survey of Iraq from 1978 to 1980 and as a postdoctoral fellow from 1984 to 1986, and then, he worked as assistant professor (1986–1988) at the University of Ottawa. He joined the University of Windsor in 1988, and he is now a Full Professor, and served as head of the Department of Earth and Environmental Sciences, University of Windsor from 2004-2010. He is currently on leave and affiliated with the Petroleum Institute of Abu Dhabi, UAE. His principal area of research is on petrologic and chemical attributes of carbonate and siliciclastic diagenesis, dolomitization, and environmental geochemistry. He has published over 80 peer-reviewed papers in national and international journals and over 120 conference abstracts. For the past 15 years his research focus has been on dolomitization and reservoir characterization in WCSB and other world basins. In particular, he focused on the role of hydrothermal dolomitization and reservoir evolution. He acted as an Associate Editor for the Journal of Sedimentary Research and Journal of Marine and Petroleum Geology and holds memberships in AAPG, SEPM, the Geological Association of Canada, and the International Association of Sedimentologists.*

ialaasm@pi.ac.ae

Fadi H. Nader *is currently on a temporary leave from IFP Energies nouvelles (France) and works as a geology consultant at the Lebanese Ministry of Energy and Water within the framework of the first Lebanese offshore gas exploration bidding round project. In 2003, Fadi obtained a PhD in sedimentology from KU Leuven, Belgium. He joined the Department of Geology at the American University of Beirut as an Assistant Professor from 2003 to 2006. Since then, he works as a Research Engineer at IFP Energies nouvelles. He managed several research projects on reservoir characterization and basin analyses and supervised several MSc, PhD and Post-doctoral projects. Fadi is an active member of the American Association of Petroleum Geologists and a Fellow of the Geological Society, London. His research interests are petroleum exploration, reservoir characterization and modeling as well as basin studies.*

adi-henri.nader@ifpen.fr

Andrea Ceriani *is a Senior Lecturer of Petroleum Geology and Sedimentology at the University of Pavia, Italy. He received his MSc (1995) and PhD (2001) degrees from the same institution. His current research includes sedimentology and petrography of carbonates and siliciclastics, particularly focused on carbonate and sandstone diagenesis. His main interest is in the application of aqueous and hydrocarbon fluid inclusions to study the diagenetic and thermal history of reservoir rocks, the evolution and migration of fluids in sedimentary basins, and to define history of migration and type of hydrocarbons.*

andrea.ceriani@unipv.it

Marta Gasparrini *joined IFP Energies nouvelles in 2009. She obtained her PhD in Geology from the University of Heidelberg in Germany (2003). She also worked as Research-Sedimentologist for the University of Naples, Italy and the INGV – National Institute for Geophysics and Volcanology, Italy. She mainly addressed her research into developing conceptual models in diagenesis and hydrothermal alteration of carbonates.*

marta.gasparrini@ifpen.fr

Howri Mansurbeg *is a Petroleum Geologist with particular expertise in diagenesis, sequence stratigraphy, and reservoir characterization of siliciclastics and carbonates. He has obtained his PhD from Uppsala University, Sweden, in 2007. His current research deals with hydrocarbon exploration and exploitation in carbonate reservoirs in Iraqi Kurdistan utilizing an integrated multidisciplinary approach. Howri has worked for several international oil companies in Europe and the US and has produced many technical reports and research articles in the past 10 years. He is currently an Associate Professor at the Department of Petroleum Geosciences and also Vice President for Scientific Affairs at Soran University in the Iraqi Kurdistan.* *howri.mansurbeg@gmail.com*

Manuscript received May 12, 2011

Revised October 13, 2011

Accepted November 30, 2011